Electronic approaches to restoration of sight

2016 Rep. Prog. Phys. 79 096701

(http://iopscience.iop.org/0034-4885/79/9/096701)

IOP Publishing Reports on Progress in Physics
Rep. Prog. Phys. 79 (2016) 096701 (29pp) doi:10.1088/0034-4885/79/9/096701

Review

Electronic approaches to restoration of sight

G A Goetz[1,2] and D V Palanker[1,3]

[1] Hansen Experimental Physics Laboratory, Stanford University, Stanford, CA 94305, USA
[2] Neurosurgery, Stanford University, Stanford, CA 94305, USA
[3] Ophthalmology, Stanford University, Stanford, CA 94305, USA

E-mail: ggoetz@stanford.edu and palanker@stanford.edu

Received 11 November 2014, revised 11 April 2016
Accepted for publication 23 May 2016
Published 9 August 2016

Abstract

Retinal prostheses are a promising means for restoring sight to patients blinded by the gradual atrophy of photoreceptors due to retinal degeneration. They are designed to reintroduce information into the visual system by electrically stimulating surviving neurons in the retina. This review outlines the concepts and technologies behind two major approaches to retinal prosthetics: epiretinal and subretinal. We describe how the visual system responds to electrical stimulation. We highlight major differences between direct encoding of the retinal output with epiretinal stimulation, and network-mediated response with subretinal stimulation. We summarize results of pre-clinical evaluation of prosthetic visual functions *in-* and *ex vivo*, as well as the outcomes of current clinical trials of various retinal implants. We also briefly review alternative, non-electronic, approaches to restoration of sight to the blind, and conclude by suggesting some perspectives for future advancement in the field.

Keywords: brain-machine interface, retinal prosthesis, neural prosthesis, electrical stimulation, neural stimulation, retina, phosphene

(Some figures may appear in colour only in the online journal)

1. Introduction

Retinal degenerative diseases resulting in the progressive loss of photoreceptors are among the leading causes of incurable blindness today [1]. Retinal prostheses are designed to reintroduce visual information into the neural system by stimulating the surviving retinal neurons electrically. Several such systems are already in clinical trials, and more advanced technologies are being developed. This review summarizes various approaches to retinal implants, and discusses the challenges and perspectives associated with electronic restoration of sight.

1.1. Extracellular electrical stimulation as an input into the nervous system

Neural activity can be affected by modulating the membrane potential of neurons using electric currents, which can be delivered intra- or extra-cellularly.

Intra-cellular electrical stimulation is relatively well understood and widely used in laboratory settings for characterizing the electrical properties of cells. The two classical models for intracellular stimulation, described by the Weiss and Lapicque equations, are computationally simple and supported by a wealth of experimental measurements [2, 3] (see section 3.2). However, direct access to the cell cytoplasm is difficult and very invasive, which makes it impractical for chronic use. Developing approaches for less invasive integration of nano-electrodes with cells remains an active topic of research [4].

So far, all electro-neural interfaces used for therapeutic and diagnostic applications have relied on extracellular access to the cells for both stimulation and recording. Although theoretical models for extracellular stimulation are much more complex than those for intracellular stimulation, and mechanisms of neural network activation less understood, there is ample experimental evidence for efficacy of extracellular electrical stimulation. In the central nervous system, devices

that make use of it range from deep-brain stimulators for alleviating symptoms associated with Parkinson's disease, dystonia and others [5] to sensory prostheses such as cochlear [6] or retinal implants [7]. There are also multiple interfaces for the peripheral nervous system, including sacral nerve stimulation for bladder control [8], lacrimal gland stimulation for secretion of tears in dry eye disease [9], and many others.

Extracellular stimulation works by polarizing cells in a gradient of potential created by electric currents in the extracellular medium. The highly conductive cell cytoplasm, surrounded by a poorly conducting membrane, rapidly becomes equipotential. This results in a decrease in trans-membrane potential (also called a depolarization) in some regions, while other regions are concurrently hyperpolarized. Spatial distribution of the hyperpolarized or depolarized areas depends strongly on location and orientation of the cell relative to the stimulating electrodes and their geometry [10, 11]. The effect of such changes in trans-membrane potential on neural activity further depends on the distribution of the voltage-sensitive ion channels over the cell membrane and on their kinetics [12]. Therefore, pulse polarity, amplitude and duration need to be chosen with care to achieve the desired effects, as well as the placement, size and shape of the stimulating electrodes. These considerations are discussed in section 3.2.

1.2. Cochlear implants: an exemplary success of neuroprosthetic sensory restoration

Successful restoration of hearing to the deaf with cochlear implants is the most striking example of the potential of prosthetic sensory rehabilitation. The rigorous, principled and well-developed approach to sensory restoration undergone by cochlear implants can serve as an example for retinal prostheses.

The structure of the inner ear is such that different frequencies of sound waves cause sensory neurons, known as hair cells, to vibrate in different regions of the cochlea. While high frequencies are detected at the base of the cochlea, lower frequencies elicit responses deeper in the cochlea. Hair cells then transmit information about the spectral composition of the sound waves via the spiral ganglion cells and the auditory nerve to the auditory cortex.

Patients with severe damage to their hair cells are profoundly deaf, but the next layer of neurons in their auditory system—the spiral ganglion cells making up the auditory nerve fibers—usually remains intact, just as the inner and ganglion cell layers of the retina remain relatively intact in retinal degenerations (see section 1.4.2). Electrical stimulation of the spiral ganglion cells by electrodes distributed along the cochlea can elicit percepts of sounds, and cochlear implants function well enough to enable speech recognition [6]. They are widely used to alleviate auditory loss in adults and children alike, with more than 320,000 total implantations world-wide as of December 2012.

A modern cochlear prosthesis consists of the following modules: one or several external microphones pick up sounds from the environment and relay them to a speech processor, which usually prioritizes audible speech in the signal, and filters out other components. The speech processor then passes on the signals by electromagnetic induction to an implanted receiver and stimulator, which drives electrical impulses in an array of electrodes. The intra-cochlear array consists of 12–20 electrodes distributed along a thin cable that follows the shape of the patient's cochlea.

Despite a massive reduction in the number of channels transmitting auditory information: no more than 20 electrodes for 30,000 axons in the auditory nerve, the success of cochlear implants has been astounding, and it can be linked to two key elements. First, the electrode arrays deliver stimuli matched to the natural encoding scheme of the auditory system, as they are designed to independently stimulate different areas of the cochlea that encode different spectral components of the sound waves. Second, pre-processing modules simplify the incoming auditory signals, which can thus be better encoded with just a few electrodes in a diseased cochlea. For example, pre-processing has enabled patients to recognize speech. We expect that such design decisions will be even more important with retinal prostheses, since the interface is two dimensional and intra-retinal signal processing is more complex.

1.3. Visual processing in the retina

The success of cochlear implants has inspired scientists and clinicians to try restoring vision in blind patients by electrical stimulation of the neurons that relay visual signals to the brain. Vision begins with the projection of spatio-temporal patterns of incident light by the cornea and lens onto a thin layer of tissue lining the back of the eye, called the retina (figures 1(a) and (b)). This light-sensitive extension of the central nervous system consists of three neural layers: the photoreceptor layer, the inner nuclear layer and the ganglion cell layer.

Photoreceptors are graded-response neurons (i.e. they do not generate action potentials) that transduce photons into changes in their membrane potential by means of light-sensitive proteins called opsins. The vertebrate retina is inverted, so that photoreceptors are located at the back of the eye in contact with the retinal pigment epithelium (RPE), which is essential to the health and function of the photoreceptors. RPE cells regenerate photopigments and digest outer segments shed by the photoreceptors. Without support from the RPE, photoreceptor cells progressively atrophy and die.

The human retina contains about 120 million photoreceptors. Cones dominate the central regions of the visual field and are responsible for day vision. Rods dominate the periphery and mediate night vision. Primates and humans have three distinct cone subtypes in their eyes, called S, M and L (for short, medium and long wavelength) cones [13]. S cones are mostly sensitive to the blue component of the visible light spectrum. M and L cones have significant spectral sensitivity overlap, with M cones exhibiting peak sensitivity in the middle of the visible light spectrum, and L towards the longer end of the spectrum [13].

Photoreceptors relay visual information to the neurons in the inner nuclear layer of the retina, where 2 types of horizontal cells, about 12 types of bipolar cells, and as many as 30 types of amacrine cells [14, 15] process the visual signals.

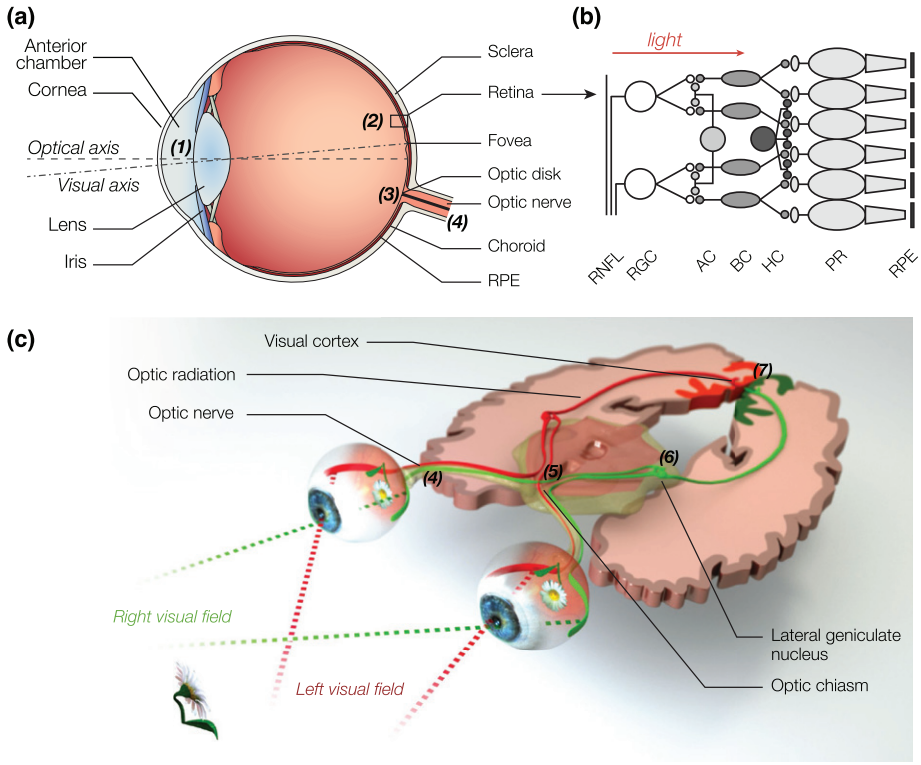

Figure 1. The human visual system. (a) Visual perception begins in the eye, where the cornea and lens (1) project an inverted image of the world onto the retina (2), which converts incident photons into neural action potentials. (b) The retina consists of three layers of cells. The photoreceptors (PR), which are in contact with the retinal pigment epithelium (RPE), convert light into neural signals that propagate to the horizontal (HC), bipolar (BC) and amacrine cells (AC) of the inner nuclear layer. The axons of the retinal ganglion cells (RGCs) form the retinal nerve fiber layer (RNFL). They converge onto the optic disk (3), where they congregate to form the optic nerve (4), which relays neural signals to the brain. (c) Signals from the left and right visual fields of both eyes are combined at the optic chiasm (5). The lateral geniculate nucleus (6) relays the left visual field to the right visual cortex and the right visual field to the left visual cortex through neuron axons called the optic radiation. Higher visual processing finally takes place in the visual cortex (7), and further downstream in the brain.

Retinal interneurons are primarily non-spiking, even though some amacrine cells can produce action potentials [16]. Retinal interneurons pass on visual information to over 30 distinct classes of retinal ganglion cells (RGCs) [17] that generate action potentials relayed to the brain by their axons, which constitute the optic nerve (figure 1(c)). There are approximately 1 million RGC axons in the human optic nerve [18].

RGCs encode visual information over a spatially limited region called their receptive field, which consists of a central area called the center, and a surrounding ring called the surround. Retinal ganglion cells that respond to increments of light over the center of their receptive field are called ON ganglion cells, while the ones that respond to light decrements over the center are called OFF ganglion cells. The surround is antagonistic to the center, which means that ON-center ganglion cells have OFF surrounds, and vice versa. Ganglion cells can also have spectral opponency properties, such as the blue-ON center, yellow-OFF surround small bistratified cells [19]. In the primate retina, midget ganglion cells have been hypothesized to be responsible for high acuity vision, and the parasol ganglion cells project to areas of the brain thought to encode motion [20–22]. In other species, such as the rabbit, rat or mouse, direction-selective ganglion cells respond to visual motion in a preferred direction [23, 24], and object-motion sensitive cells are able to segregate motion of objects from that of a background [25].

Bipolar cells relay visual information from the photoreceptors making up the center of the receptive field to the ganglion cell. Horizontal cells are involved in contrast adaptation, and mediate part of the antagonistic center-surround effect. Amacrine cells are also involved in center-surround effects by providing lateral inhibition in the retinal network. Starburst amacrine cells are at the heart of the motion direction-selectivity tuning [26]. The role of many other amacrine cell types in shaping complex retinal computations is still under debate in the visual neuroscience community.

1.4. Blindness and its effects on the visual system

1.4.1. The main causes of blindness. The leading cause of incurable blindness in the developed world today is a broad category of diseases known as retinal degenerations [1, 27]. In these conditions, the photoreceptors progressively die, eventually leading to loss of sight. However, neurons in the inner nuclear and ganglion cell layer survive to a large extent (see section 1.4.2) and can be stimulated electrically, making them good targets for retinal prostheses.

Age-related macular degeneration (AMD) primarily affects older patients: onset of the disease typically takes place after 60 years of age. As AMD progresses, the retinal pigment epithelium cells deteriorate, forming cellular debris called

drusen between the pigment epithelium and Bruch's membrane, which separates the RPE from the choroid. Drusen are thought to impede the transport of nutrients from the choroid, and tend to grow over time.

Eventually, in the dry form of AMD, RPE cells in the center of the visual field can begin to atrophy, which leads to the death of the photoreceptors above them. This condition is called geographic atrophy, and it results in the formation of a central blind spot, called a scotoma.

Alternatively, new blood vessels may start growing from the choroid into the retina, which degrades central vision. This process is called neovascularization, also known as wet AMD. Anti-angiogenic drugs can block the signaling pathway of the vascular endothelial growth factor (VEGF) and thereby prevent neovascularization. These anti-VEGF molecules, injected directly into the vitreous humor of the eye, have a rather short lifetime in the body (weeks), and need to be delivered on a monthly basis to prevent growth of new blood vessels.

Both forms of AMD affect photoreceptors in the central area of the visual field, called the macula, and leave peripheral vision relatively intact. People suffering from AMD have difficulties with tasks requiring high visual acuity, such as reading or face recognition, but their remaining peripheral vision usually enables good ambulation without walking canes or guide dogs.

Retinitis pigmentosa is a broad class of genetic disorders which typically affects patients in their twenties or thirties, with an incidence rate of approximately $1:4000$ [1]. This inherited disease typically begins with a loss of rod photoreceptors in the periphery, and eventually leads to a loss of the remaining cone photoreceptors in the center. As the disease progresses, patients start suffering from tunnel vision, with some bare light perception in the periphery, and central light sensitivity can eventually disappear as well.

The majority of retinitis pigmentosa patients retain some degree of sight [28], and since the spatial resolution provided by retinal prostheses has so far been extremely low, only profoundly blind patients (characterized by bare light sensitivity and below) can be considered candidates for implants today. Retinitis pigmentosa is a prime candidate for gene therapy, and several clinical trials are in progress. However, due to the large variability in genetic defects that can lead to this condition, it is unlikely that one single cure for all its forms will be found.

Blindness and visual acuity. Both retinitis pigmentosa and age-related macular degeneration are characterized by a significant loss in visual acuity—one of the most important characteristics of visual function, which quantifies spatial resolution. Typically, it is measured by assessing the patient's ability to discriminate between objects on standardized charts. In the United States, visual acuity is most commonly measured in units of $20/x$. LogMAR (for LOGarithm of the Minimum Angle of Resolution), another unit for visual acuity, is defined as the negative decadic logarithm of the fractional visual acuity, so that the logMAR acuity is $-\log(20/x) = \log(x/20)$.

20/20 is considered normal visual acuity, and corresponds to the ability to resolve lines 1.75 mm apart from a distance of 20 feet. This object size corresponds to a visual angle of 1 min of arc, or 5 micrometers on the retina. Having a visual acuity of $20/x$ then means that one sees from 20 feet away an object equally well as a person with normal visual acuity would x feet away. A visual acuity of 20/10 is therefore twice better than normal, and a visual acuity of 20/40 twice worse than normal. People with a visual acuity of less than 20/200 are considered legally blind in the United States, while the World Health Organization sets the limit at 20/400. In countries that use the metric system, the distance is expressed in meters, and since 20 feet is about 6 meters, the units of visual acuity are $6/x$.

Visual acuity is a perceptual notion, and reporting it in units of $20/x$ implies perceptual equivalence between what two subject see. However, since the percepts elicited by visual prostheses are inherently very different from natural vision, it would be misleading to imply such equivalence. Therefore, it is important to keep in mind that even though spatial resolution of prosthetic vision is assessed in these units, these numbers reflect only spatial frequencies resolvable by the implanted patient, and not many other aspects of visual function.

Field of view. Importantly, the definition of legal blindness in the United States includes not only visual acuity below 20/200, but also a visual field below 20 degrees in the better seeing eye. To restore functional vision, retinal implants should therefore aim at providing a sufficiently large field of view for comfortable orientation and ambulation, ideally exceeding 20 degrees.

1.4.2. Effects of retinal degeneration on the retinal network.

While retinal degenerations leave the inner nuclear layer and ganglion cells relatively intact for extended periods of time [29], significant changes in retinal organization can take place at the end phases of the disease, when the vast majority of the photoreceptors are lost [30–32] (see figure 2(c)). These changes are broadly called retinal remodeling. During this process, amacrine and bipolar cells can migrate either to the distal retina or to the ganglion cell layer. While all neurons appear to retain their normal basic molecular signatures, new synaptic connections are abundant. In the final stages of retinal remodeling, neuronal death can significantly deplete the inner nuclear and ganglion cell layers, with glial cells partially filling the space left by deceased neurons [30, 31]. These changes are likely to significantly impact retinal signal processing and neural activity, and therefore will influence our ability to encode visual information with a prosthetic interface.

AMD patients are less likely to suffer from extensive remodeling than retinitis pigmentosa patients since (1) the onset of the disease is much later in life, and (2) the peripheral retina is preserved, which could help maintain more normal neural activity in the center via lateral connectivity in the retinal network.

There are multiple models of retinal degeneration in rodents (mice and rats), pigs, and cats [30]. Various deficiencies in the RPE and photoreceptors in these animal models result in different time courses of degeneration and in varying extent of cellular preservation. Animal models of retinal

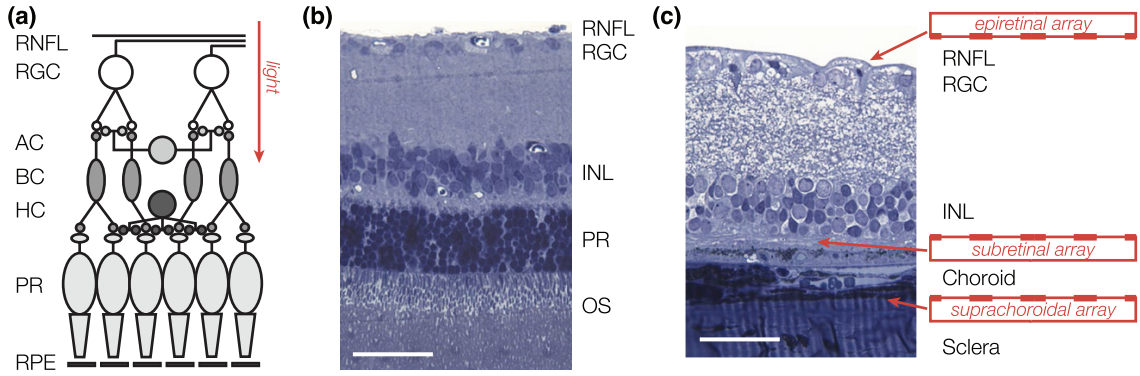

Figure 2. Implant placement. (a) Simplified wiring diagram of the retina. Signals from the photoreceptors (PR) are processed and relayed by the horizontal (HC), bipolar (BC) and amacrine cells (AC) of the inner nuclear layer (INL) to the retinal ganglion cells (RGC). The axons of the retinal ganglion cells form the retinal nerve fiber layer (RNFL), which relays visual signal to the brain. Photoreceptors are located at the back of the eye, in contact with the retinal pigment epithelium (RPE). (b) Histology cross-section of a healthy rat retina. RNFL: retina nerve fiber layer; OS: photoreceptor outer segments. Scale bar: 50 μm. (c) Epiretinal implants are in contact with the ganglion cell layer of the retina, while subretinal implants approach the retina from the photoreceptor side. In a degenerate rat retina, as shown here, subretinal implants are in direct contact with the inner nuclear layer. Suprachoroidal implants are placed on the other side of the choroid, above the sclera. Scale bar: 50 μm.

degeneration used for research in retinal prosthetics are discussed in section 3.1.

2. Approaches to retinal prosthetics

2.1. Placement of the stimulating electrodes

Depending on their location in the patient's eye, retinal implants fall into one of three categories: epiretinal, subretinal or suprachoroidal.

In the epiretinal approach, prostheses target primarily the retinal ganglion cells, using electrodes placed on top of the inner limiting membrane (figure 2) [33, 34]. RGCs respond to sub-ms stimuli by generating an action potential within about a millisecond. Multiple stimuli can be used to generate bursts of spikes, encoding visual information. Epiretinal implants can activate RGCs at frequencies exceeding 100 Hz, and they typically encode stronger percepts using higher frequency stimulation (see section 3.4.1). Epiretinal devices usually bypass the inner nuclear layer of the retina, and can therefore elicit retinal response as long as RGCs survive. They can be implanted with relative ease, and can also be easily explanted in case of post-surgical complications, or of failure of the device.

In the subretinal approach, arrays of electrodes located between the inner nuclear layer and the pigment epithelium replace the degenerated photoreceptor layer and target primarily the surviving bipolar cells (figure 2) [7, 35]. Subretinal implants deliver visual information to non-spiking inner retinal neurons, and stronger stimuli are encoded with larger amplitude or longer duration pulses (see section 3.4.2), rather than higher frequency pulse trains used for direct encoding in the RGCs. Signals are converted into action potential trains in the ganglion cells via synaptic connections in the retinal neural network. Implanting a subretinal device is more difficult than implanting an epiretinal device: the surgical procedure involves the creation of a local retinal detachment and a small retinal or trans-scleral incision, through which the device is placed into the subretinal space, after which the retina is reattached. Excessively traumatic implantations can lead to fibrosis and scaring. In the case of wired subretinal implants, large areas of the retina need to be detached during implantation, which is a significant challenge with fragile diseased retinas. Explanting a subretinal device is also significantly more difficult than epiretinal, although it has been done with the Alpha IMS implant (section 4.3). Explantability of photovoltaic subretinal devices (section 2.2.3) remains to be demonstrated.

In a third approach, called suprachoroidal, the implant is placed between the choroid and the sclera (figure 2). While it has been suggested that this approach is surgically less risky than both epi- and subretinal prostheses [36, 37], the large distance between stimulating electrodes and retinal neurons greatly restricts attainable spatial resolution. Therefore, such implants are placed in the periphery of the visual field, and are designed to help with low-resolution peripheral vision, primarily for ambulation.

Changes in the retinal network that take place during retinal degeneration (section 3.1) are likely to significantly impact retinal signal processing and neural activity, and therefore will influence our ability to encode visual information with any prosthetic interface. Subretinal prostheses are particularly vulnerable in this regard, since they rely on connections between the inner retinal neurons and the ganglion cells. For epiretinal prostheses, the abnormally high spontaneous firing rate of ganglion cells frequently observed in animal models of retinal degeneration also represents a problem, since it will likely impede the ability of the implant to encode a desired sequence of spikes.

2.2. Delivery of information and power to the implant

Transfer of information and power to the implant is a challenging engineering problem, since direct connection of an

implant to external electronics via a transcutaneous wire is prone to infections and severe scarring [38]. Therefore, in modern implants, it is done wirelessly, using one of the following techniques: (1) delivery of power and serial telemetry of the data through inductive coils, (2) optical transmission of the data with power delivery through inductive coils, or (3) optical delivery of data and power to the implant.

2.2.1. Serial telemetry of the data. Inductive coils are widely used to transmit power and data to medical devices, such as for example cochlear implants and retinal prostheses. In such systems, an AC current driven through an external transmitting coil induces an AC current in the implanted receiving coil, which is converted into DC current in the implant. The transmitting and receiving coils are typically weakly coupled [39], with the coupling coefficient k in the range 0.08–0.24, much lower than in normal transformers, where $k \sim 0.9$.

A capacitor in series with the receiving coil creates a tuned resonance at the transmitter frequency f, and the resulting circuit amplifies the received voltage by a quality factor Q, typically in the range 10–100. Quality factor increases with frequency, however RF absorption in tissue increases exponentially beyond a few MHz [40], limiting the range of useful frequencies to below a few MHz.

Unfortunately, while a high Q coil is efficient for receiving power, it is a rather poor data receiver, which makes it challenging to use a single coil for both data and power. According to the Shannon-Hartley theorem [41], the data capacity C of a coil can be expressed as:

$$C = \frac{f}{Q}\log(1 + \mathrm{SNR}) \tag{1}$$

where C is in bits s^{-1} and f/Q is the bandwidth of the circuit, inversely proportional to the quality factor. SNR in this equation is the signal-to-noise ratio of the transmitted signal.

For this reason, one coil is often used for power and another for data [39], with data transmitted at a higher frequency and with a lower quality factor coil. Efforts have been put towards developing single receiving coil systems with high Q, that can also efficiently deliver data, and one such system achieved transmission rates above 1 MB s^{-1} [42].

In terms of data bandwidth requirements, the maximum number of pixels N that can be driven at a refresh rate R with S stimulation (gray) levels is:

$$N = \frac{C}{R\log_2 S} \tag{2}$$

so that a data rate of 1 MB s^{-1} can support $64 \times 64 = 4096$ pixels with a refresh rate of 60 Hz and 16 grey levels in the image.

Visual information transmitted from the camera to the implant via serial telemetry does not depend on eye movements, which creates two problems. (1) The brain expects images to shift on the retina during eye movements. In particular, stationary objects should translate with the changing direction of gaze. Since the stimulation patterns in such implants do not shift with the eye movement, the brain interprets this as motion. Similar effects have been reported with cortical visual prostheses [43]. To avoid this phenomenon, patients are asked to keep their direction of gaze steady. (2) Instead of using natural eye scanning, patients are required to scan the visual field with their heads—a very unnatural paradigm. These limitations could be alleviated by incorporating an eye tracker in the system, which would shift the image delivered to the implant according to the direction of gaze.

It is difficult to scale coil-based designs to thousands of electrodes for two reasons: (1) doing so requires a very wide data bandwidth, (2) wiring of thousands of electrodes makes the cable quite rigid and the feed-through rather bulky. Multiplexing the signals on the array itself would reduce the required number of wires, but it adds electronics to the retinal array itself, which affects its weight and flexibility.

A number of retinal implants make use of coils for data and power transmission. The Argus II epiretinal prosthesis (Second Sight Medical Systems, Sylmar, CA, USA) uses such a coil-based design, and it has been approved by the FDA as a Humanitarian Use Device (see section 4.2). The Boston Retinal Implant [44] and the EPIRET3 implants [45] also use serial telemetry to deliver power and data to the implant.

2.2.2. Powered implants with integrated cameras. A few designs have been proposed that deliver only power through inductive coupling, and transmit visual information through the natural optics of the eye [7, 46]. The best known of these systems is the Alpha IMS implant, developed by Retina Implant AG (Reutlingen, Germany) (see section 4.3). Their subretinal implant is a camera with an active circuitry and stimulating electrode in each pixel that converts incident images into electrical stimulation patterns on the electrode array. The Alpha IMS implant was designed to operate under typical daylight illumination conditions. It includes a subdermal power receiving coil placed behind the ear, similarly to cochlear implants. Power is then routed to the subretinal implant via a trans-scleral cable.

Implants with integrated cameras very efficiently receive visual information, and they naturally couple eye movement to the stimulation pattern on the implant. However, the cable connecting the retinal implant to the extraocular power supply makes the implantation procedure difficult, long, and prone to complication. In the case of the Alpha IMS implant, developing a flexible and robust trans-scleral cable and feed-through that withstands the effects of eye movements over the long term remains a challenging engineering problem.

2.2.3. Photovoltaic systems. The third category of retinal implants receives both data and power by light, via the natural optics of the eyes [47, 48]. These implants directly convert incident light into electric current to stimulate the nearby neurons (figure 3).

Using an array of photodiodes as a subretinal implant was first proposed in the 90s [50]. In that design, the photovoltaic pixels consisted of single photodiodes, and the implant was expected to convert ambient illumination into stimulating currents. However, ambient light on the retina is much too dim for photovoltaic stimulation [51]. In addition, photovoltaic conversion of continuous illumination cannot provide

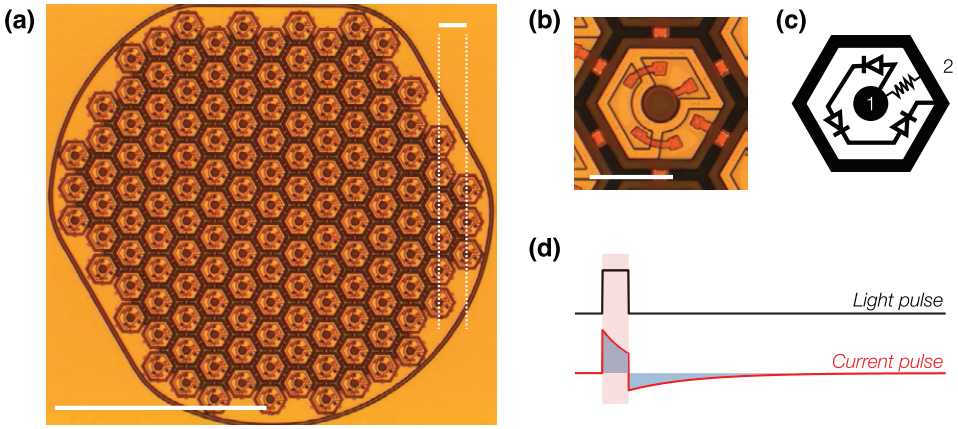

Figure 3. Subretinal photovoltaic implant. (a) A single module of a photovoltaic prosthesis, which consists of 70 μm-wide pixels separated by 5 μm trenches arranged in a 1 mm-wide hexagonal pattern. Scale bar: 500 μm, bottom left; 65 μm, top right. (b) Close-up photograph of an anodic 70 μm-wide pixel. Scale bar: 50 μm. (c) The wiring diagram for a pixel. Each pixel consists of two to three (shown here) photodiodes connected in series between the central active (1) and surrounding return (2) electrode. (d) In the absence of irreversible Faradaic reactions, a light pulse is converted by the implant into a charge-balanced current pulse flowing through the inner retina. Adapted with permission from [49], copyright Nature 2015.

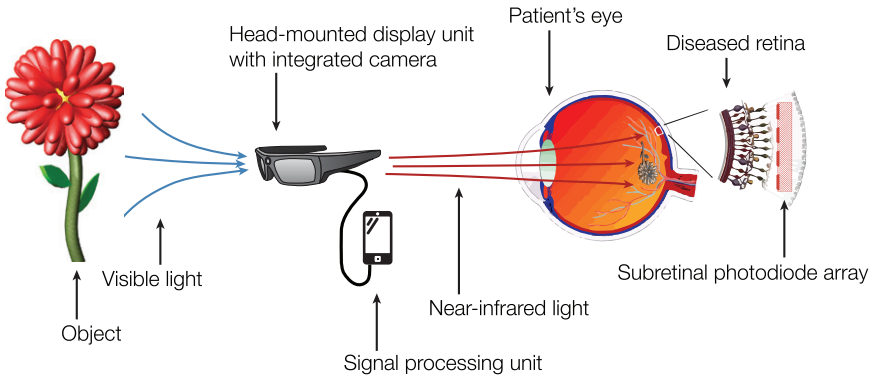

Figure 4. Concept of a fully optical photovoltaic retinal prosthesis. A head-mounted camera captures visual scenes, which are processed by a mobile signal-processing unit. High-power near infrared light relays visual information to a photovoltaic subretinal implant through the natural optics of the eye.

charge-balanced current pulses, which are required to avoid hydrolysis and electrode erosion.

A revised concept of a photovoltaic subretinal implant powered by intense pulsed light projected from video goggles was proposed in 2005 [51], first implemented in 2007 [46], and has been actively developed since then [47, 49]. Intense illumination can be provided by a near-the-eye display [52], similar to conventional video goggles, apart from its significantly higher irradiance. A pocket computer provides a convenient means of processing images prior to displaying them onto the implant (figure 4). In order to avoid photophobic and phototoxic effects of bright illumination, photodiode-based systems can use near-infrared (850–915 nm) wavelengths, which is invisible to the remaining photoreceptors.

The photocurrents created by the implant increase linearly with light intensity, until saturation is reached at a level defined by the ratio of the maximum photovoltaic voltage to the tissue impedance. Adding photodiodes in series helps increase this maximum voltage, but pixels then require more light since incident light is divided between the photodiodes in each pixel. Two diodes per pixel was found to be the optimal configuration for subretinal stimulation [53].

Instead of crystalline silicon, photovoltaic elements based on light-sensitive polymer films have also been proposed [48].

An attractive feature of photovoltaic systems is that they do not require any wires [47, 49]. Therefore, an implant can consist of a large number of independent modules that tile the visual field. These modules can be inserted into the subretinal space via a small incision and follow the curvature of the eye, making the surgery minimally-traumatic [54].

2.3. Safety considerations

2.3.1. Implant encapsulation. Exposure of an implant to body fluids can lead to its erosion and eventual failure. Implants can also trigger strong tissue reaction if they are not properly encapsulated in biocompatible materials. This may lead to formation of a glial or fibrotic seal around the implant, which will increase both the distance between electrodes and target neurons and impedance of the stimulating electrodes [55].

For these reasons, electronics in the majority of neural implants are enclosed in metallic or ceramic containers, with feed-through connectors to the power source and electrode array. The resulting implant is hermetically isolated from corrosive body fluids, stable, but bulky. Surgical procedures then involve placing different modules (coil, power and data-processing electronics as well as the electrode array) and routing interconnecting cables in the patient [7, 34] (see section 4).

While crystalline silicon implants are well tolerated over the short term [56, 57], detectable degradation occurs over a year. Such implants require a stable and biocompatible layer to provide protection against water and ion ingress.

Dielectric materials deposited by low-pressure chemical vapor deposition at high temperatures (800–900 °C) have exhibited good stability *in vivo* [58, 59], however the deposition temperatures are incompatible with integrated circuits manufacturing processes. Polymers such as Parylene are used in the medical industry for encapsulation of neural implants [60, 61], but Parylene absorbs water and develops cracks [62], and therefore cannot be used for encapsulation of unprotected integrated electronic circuits. Atomic layer deposited Al_2O_3 is conformal and hermetic, and as such can provide decent encapsulation. However, it slowly dissolves in water [63]. Diamond-based coatings [64–66] and amorphous Silicon Carbide [67] deposited at low temperatures are being explored as other possible encapsulating materials for neural implants. Recent studies have provided promising results regarding biocompatibility of diamond interfaces [68]. It remains to be seen, however, whether the limited charge injection capability of these interfaces is sufficient for safe and efficient retinal stimulation. Plasma-enhanced chemical vapor deposited amorphous silicon carbide (SiC) is a promising material for encapsulating neural implants, as SiC films do not dissolve in accelerated aging tests. Care should be taken with SiC films deposited over steps and rough surfaces, as defect density then increases significantly. A combination of thermal Silicon Oxide coated with SiC could provide adequate protection of retinal implants [69].

2.3.2. Thermal limits. For both RF- and optically-powered implants, tissue heating resulting from absorption of electromagnetic radiation and energy dissipation in the implanted electronics must be kept within acceptable safety limits. ISO norm 14708-1 article 17.2 specifies that temperature rise in chronic operation should not exceed 2 °C, since this is within the natural range of body temperature variation.

The heating induced by the implant is governed by the following equation [70], which can be solved numerically using finite element models:

$$\rho c_p \frac{\partial T}{\partial t} = \nabla(k\nabla T) + Q(x,t) - A_p(x)\rho_b c_b(T - T_0) \quad (3)$$

where ρ and c_p are the density and heat capacity of the medium, k is the thermal conductivity, Q is the volumetric heat source term, A_p is the local blood perfusion rate, ρ_b and c_b are the density and heat capacity of the blood, and T_0 is the arterial temperature, often assumed to be the same as the baseline body temperature, 37 °C.

For optical implants, the use of bright illumination is a safety concern. Visible and near-infrared (below ~900 nm) light is absorbed primarily by pigmented tissues, such as the retinal pigment epithelium, with a practically negligible absorption (<0.06 cm^{-1}) in transparent ocular layers such as the cornea, lens, and neural retina. Ocular safety standards [71] provide some guidelines as to the maximum permissible radiant power $MP\Phi$ that may be chronically delivered to the retina:

$$MP\Phi = 6.93 \times 10^{-5} \Lambda \Theta P^{-1} \quad (4)$$

where $\Lambda = 100(\lambda - 700)$ in the 700–1050 nm range, with $\Lambda = 2.5$ at $\lambda = 905$ nm. Θ depends on the angular spread of the incident beam, and for retinal spot sizes greater than 1.7 mm in diameter is 29.3 W mm^{-2}. P is the pupil factor which models pupil constriction or dilation, and is exactly 1 for infrared wavelengths in the absence of dilating drugs. For a 905 nm wavelength, the average irradiance limit is therefore 5.2 mW mm^{-2}. It is important to emphasize that temperature increases with increasing spot size, which this standard does not take into account.

For single-pulse exposure, the peak irradiance limit in the 0.05–70 ms duration range is described by [71]:

$$MP\Phi = 6.93 \times 10^{-4} \Lambda \Theta t^{-0.25} \quad (5)$$

At 905 nm, $MP\Phi = 285t^{-0.25}$, where t is in ms and the result is in mW mm^{-2}. For example, the peak irradiance limits are 285, 202 and 160 mW mm^{-2} for 1, 4 and 10 ms pulses, respectively.

Detailed studies of retinal heating with and without silicon implants under various illumination conditions have shown that under typical use conditions, the temperature increase associated with activation of a subretinal photovoltaic implant is not expected to exceed 0.5 °C, well within the safety limits for chronic use [72].

2.3.3. Electroporation. Electrical stimulation of neural tissue has the potential to cause irreversible cellular damage [73]. One process by which damage occurs is called electroporation. Strong electric fields can produce sufficiently high trans-membrane voltage to make penetration of water into hydrophobic lipid bilayers energetically favorable, which leads to formation of nanometer-scale pores in the lipid bilayer [74]. The damage threshold current density j scales reciprocal to the square root of the pulse duration t ($j \sim t^{-0.5}$) [75].

A comparison of experimental stimulation thresholds [77] and electroporation thresholds measured on chick chorioallantoic membrane as well as in porcine and chick retina [75] is shown on figure 5 for biphasic charge-balanced pulses. Stimulation thresholds are approximately two orders of magnitude below the electroporation thresholds, leaving a wide window for safe stimulation of the retina.

2.3.4. Electrochemical limits. In addition to hyperthermia and electroporation, cellular damage can also be caused by the leaching of toxic electrode materials into the medium, or by local changes in pH. Neural stimulation electrodes have been extensively studied in recent years, and a large body of literature is available on the topic [78–80].

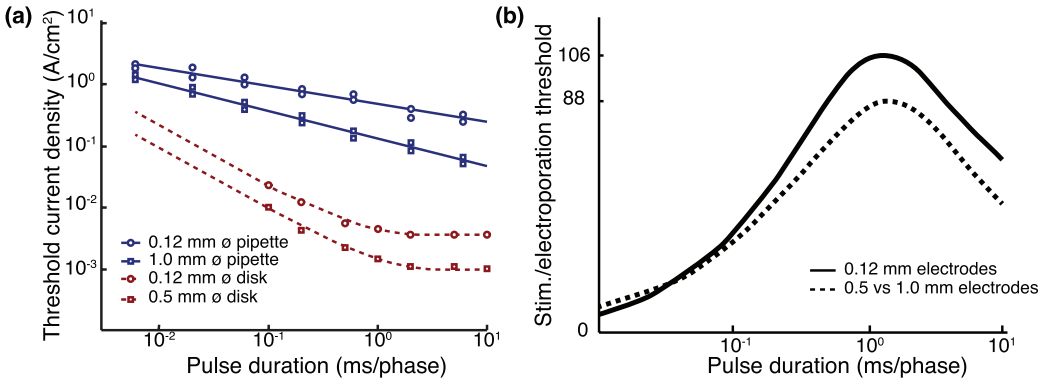

Figure 5. Thresholds for electroporation. (a) Chronic retinal damage threshold (blue curve) due to electroporation as a function pulse duration measured with pipettes 0.12 (circles) and 1.0 mm in diameter (squares). Thresholds for stimulation of ganglion cells (red curve, from [76]) are up to two orders of magnitude lower for planar disk electrodes of comparable diameters. (b) Ratio of the damage thresholds to the stimulation thresholds. Data from [75].

Electrochemical safety limits vary with electrode material and with mechanisms of charge injection, which are either capacitive or faradaic [80]. For both mechanisms, stimulation pulses need to be charge-balanced and within safe limits of the electrode potential to avoid irreversible oxidation or reduction of the electrode material as well as other irreversible electrochemical reactions. A comprehensive list of possible irreversible or harmful reactions that may take place during electrical stimulation is available in references [78, 79]. Briefly, the most common harmful processes include electrolysis of water, with consequent gas formation and changes in pH, and metal dissolution due to the formation of soluble metal complexes (especially with Pt electrodes) [80].

Capacitive electrodes are usually porous to provide a large surface area, and/or employ high dielectric constant materials, such as Titanium Nitride [81]. Faradaic charge-injection materials rely on reversible oxidation and reduction reactions to inject current. These electrodes typically provide higher charge injection than capacitive interfaces, but care should be taken in selection of the stimulation waveforms to avoid irreversible processes. The most common materials for such electrodes include Platinum and Platinum Iridium alloys, as well as activated and sputtered Iridium oxide films. Table 1 summarizes the charge injection limits of various electrode materials used in retinal prosthetics. Charge injection limits typically increase with pulse duration, especially for porous materials (not shown in table 1).

Table 1. Charge-injection limits of electrode materials for electrical stimulation of the retina.

Material	Mechanism	Max. Q_{inj} (mC cm^{-2})	Max. potential versus Ag|AgCl (V)
Pt, PtIr alloys	F, C	0.05–0.15	−0.6 to 0.8
AIROF	F	1–5	−0.6 to 0.8
SIROF	F	1–5	−0.6 to 0.8
TiN	C	∼1	−0.9 to 0.9
PEDOT	F	15	−0.9 to 0.6

Note: AIROF: Activated Iridium Oxide Film. SIROF: Sputtered Iridium Oxide Film. F: Faradaic; C: Capacitive charge injection mechanism. Adapted from [80].

3. Pre-clinical evaluation of prosthetic vision

3.1. Animal models for visual prosthetics

Retinal stimulation and characteristics of prosthetic vision have been studied both *ex vivo* and *in vivo*, in animals with normal vision and in models of retinal degeneration. The following section discusses the trade-offs associated with different animal models used for this purpose.

3.1.1. Use and limitations of the healthy retina. Animal models ranging from salamander to primates, including rodent, rabbit, cat, dog, minipig and other species, have been used in visual neuroscience to study how visual information is processed in the retina [25, 82–85]. Using healthy retina therefore makes it possible to leverage a significant body of literature about retinal responses to visual stimuli. However, it also comes with significant drawbacks, especially when studying a subretinal implant. The healthy retina has lower subretinal stimulation thresholds than degenerate tissue [47]. When working with healthy retina *ex vivo*, the stimulating electrodes are separated from the bipolar cells by a 70 μm-thick layer of photoreceptors, which is likely to increase stimulation thresholds for activation of the inner nuclear layer and reduce spatial resolution, compared to degenerate retina lacking photoreceptors [47]. In addition, electrical stimulation of the photoreceptors complicates the analysis of retinal response, as difficult pharmacological manipulations with neurotransmitter blockers are required to separate the contributions of the photoreceptors from those of the inner nuclear layer.

Some drawbacks associated with the use of healthy retinal tissue are also present in the case of epiretinal stimulation. Ganglion cells in degenerate retinas can respond to direct electrical stimulation despite severe degeneration of the photoreceptors [86–89]. However, stimulation thresholds increase in certain sub-populations of retinal ganglion cells [90], while for other sub-populations they do not change. Spontaneous RGC firing patterns change significantly with degeneration [91–93]. Hyperactivity has been reported in

many rodent animal models of retinal degeneration, including asynchronous rhythmic activation of RGCs at 7–10 Hz frequencies in the rd1 mouse retina [93]. In the rd10 mouse, RGC types with normal electrical stimulation thresholds exhibit periodic bursting [90].

Therefore, while the healthy retina is perhaps the most convenient model for comparison of natural and prosthetic retinal responses, it remains a poor proxy to degenerate tissue.

3.1.2. Rodent animal models of retinal degeneration. Researchers have developed a number of animal models of retinal degeneration to study degradation of sight associated with retinal degeneration, and restoration of vision [30]. Retinal degeneration can naturally occur in a number of species, for example mice, rats and dogs. In addition, various transgenic mice, rats and pigs, as well as knock-out mice, are also commonly used to study visual impairment. Out of these, rodent animal models are generally the most cost-effective means of carrying out animal studies.

The relevance of rodent animal models for studying visual function is under debate. For example, humans and macaques share many features in their visual systems, such as foveated trichromatic vision, well-segregated parallel pathways in the visual thalamus, ocular dominance and orientation columns in the visual cortex [94]. Rodents do not exhibit such similarity with the human visual system, but they do have an oculomotor reflex, and are capable of complex visual tasks, such as orientation discrimination [95], and invariant object recognition [96].

A well-established rat model of retinal degeneration is the Royal College of Surgeon (RCS) rat [97]. In these animals, a mutation in the receptor tyrosine kinase gene, *Mertk*, causes failure of the retinal pigment epithelial (RPE) cells to phagocytose shed photoreceptor outer segments [98], which leads to a build-up of cellular debris in the subretinal space. This, in turn, causes the progressive death of photoreceptors over a few months. By the age of 90 days (p90), the vast majority of photoreceptor outer segments are gone, and only some photoreceptor nuclei remain. By p400, photoreceptor nuclei completely disappear, while the inner nuclear layer and the ganglion cell layer remain well preserved. RCS animals are born normally-sighted, and they develop a normal visual cortex. This, combined with the relatively rapid progression of retinal degeneration—on the order of 3 months—makes them an attractive animal model for both *in vivo* and *ex vivo* studies of restoration of sight [99].

P23h and s344-ter rats are alternative rat models of retinal degenerations. In the P23h rat, both cones and rods degenerate as a result of a mutation in a rod-specific protein [100]. It takes about 300 days post-natal for scotopic (rod-dominated) vision to disappear in P23h rats, and photopic (cone-dominated) vision remains present past 450 days. The slow onset of degeneration in these animals makes it difficult to obtain tissue completely devoid of photoreceptors, making them less practical for prosthetic studies.

There are over fifteen mouse models of retinal degeneration [101], with the rate of photoreceptors loss ranging from a few days (*rd1*) to several months (*rd8* or *rd9* mice). Various models of retinal degeneration exhibit different functional properties as the disease advances, and it is unclear which of them correspond to human conditions. For example, in the *rd1* mouse, both ON and OFF RGCs exhibit hyperactivity, while in the P23h rat, only OFF cells become hyperactive in the disease. A potential drawback of mice for retinal prosthetic studies is their small eye, which makes *in vivo* studies very difficult.

3.1.3. Other models of retinal degeneration. A convenient alternative to genetic models of blindness is to cause a chronic detachment of the photoreceptors from the pigment epithelium, and thereby trigger local retinal degeneration. This can be done, for example, by chronically introducing a subretinal implant in healthy animals [49, 56, 99, 102], resulting in the degeneration of photoreceptors above the implant in a few weeks (figure 6).

Alternatively, retinal photocoagulation with a scanning laser can create a local model of retinal degeneration. Ablation of the retinal pigment epithelium (RPE) combined with direct thermal damage to photoreceptors leads to local retinal atrophy in the damaged regions, which can be several millimeters in width [102], while preserving the INL and ganglion cell layers. Selective ablation of only the RPE cells using microsecond pulses is insufficient to trigger local degeneration, since RPE cells from adjacent healthy areas rapidly migrate into the damage zone [102].

Both methods allow creating local retinal degeneration in otherwise healthy animals, and could be useful for studying the interactions between prosthetic and normal vision, as would be the case in AMD patients [103].

3.2. Electrical stimulation of the different retinal layers

3.2.1. Intracellular stimulation Intracellular activation of neurons today lacks clinical applications, as it requires chronic access to the interior of a cell. Nonetheless, since it is well described by a few equations, it can provide a good intuition regarding the mechanisms behind electrical stimulation. The following section therefore introduces two simple models for intracellular activation of a neuron.

In a resting state, the intracellular potential of a neuron is maintained by a number of mechanisms at approximately −70 mV compared to the extracellular medium. A positive inflow of ions through sodium and leakage channels is compensated by an outflow of ions through potassium channels, and ion pumps balance ionic diffusion by actively moving ions across the cell membrane. Intracellular stimulation operates by injecting a current I_S into the target cell, for example by means of a fine-tip pipette. Modeling the neuron as a RC circuit, where the capacitor represents the capacitance of the cell membrane C and the resistor limits the current of the active ion pumps which maintain the cell membrane potential (figure 7(a)) leads to the following set of equations, which describes the electrical behavior of the cell:

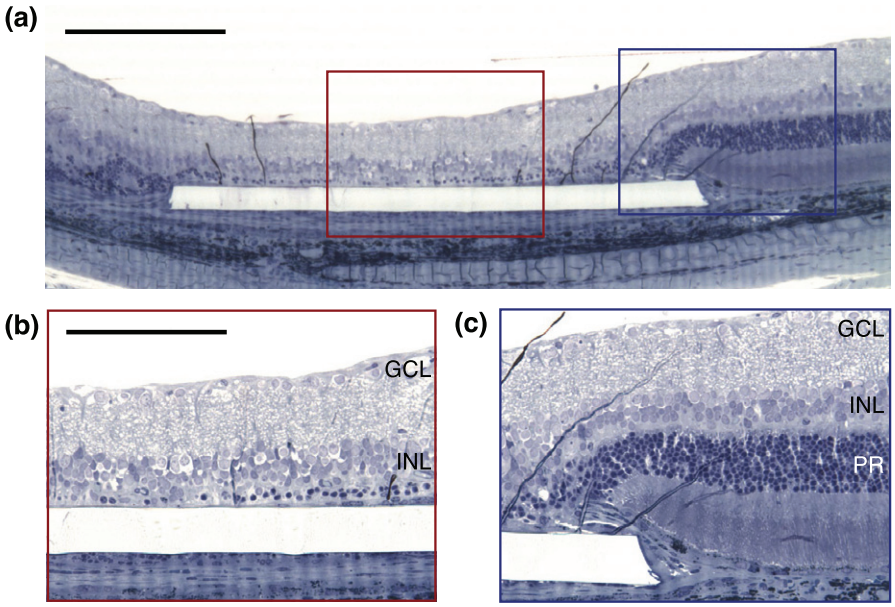

Figure 6. Local degeneration of the retina caused by a subretinal implant. (a) 5 weeks post implantation, a rat retina exhibits highly localized degeneration over the implant. Scale bar: 200 μm. (b) Above the implant, most of the photoreceptors, somas included, are gone. The inner nuclear layer (INL) and ganglion cell layer (GCL) are left intact. Scale bar: 100 μm. (c) At the edge of the implant, the retina looks healthy, and photoreceptors (PR) are present.

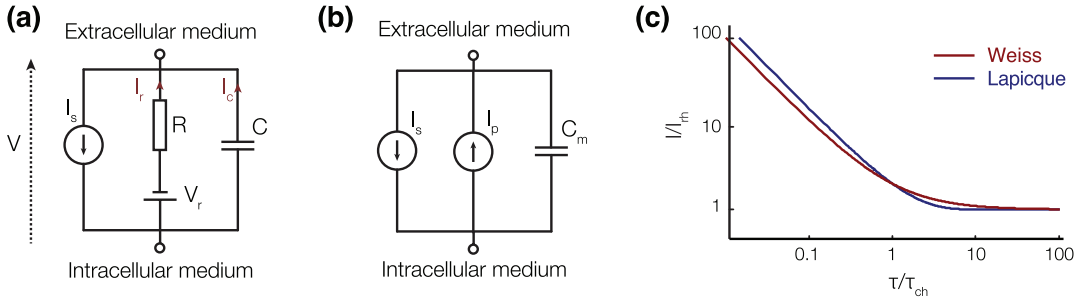

Figure 7. Equivalent circuit models of a neuron for intracellular electrical stimulation. (a) Equivalent circuit for the Lapicque strength-duration relationship. (b) Equivalent circuit for the Weiss strength-duration relationship. (c) Qualitative representation of the Lapicque and Weiss strength-duration relationships.

$$\begin{cases} I_s = I_r + I_c \\ I_r = \dfrac{V - V_r}{R} \\ I_c = C\dfrac{\mathrm{d}V}{\mathrm{d}t} \end{cases} \tag{6}$$

From these equations we can derive the minimum current I_{th} to be injected into the cell over a duration τ to bring the membrane potential to a value V_{th}:

$$I_{\mathrm{th}} = \frac{(V_{\mathrm{th}} - V_r)/R}{1 - \mathrm{e}^{\frac{-\tau}{RC}}} \tag{7}$$

where V_r is the membrane resting potential. If we define the rheobase current $I_{\mathrm{rh}} = \frac{V_{\mathrm{Th}} - V_r}{R}$ and the chronaxie time $\tau_{\mathrm{ch}} = \frac{RC}{\ln(2)}$, this equation becomes:

$$I_{\mathrm{th}} = \frac{I_{\mathrm{rh}}}{1 - 2^{\frac{-\tau}{\tau_{\mathrm{ch}}}}} \tag{8}$$

known as the Lapicque equation, after the French scientist who first carried out this derivation [104].

If V_{Th} is the threshold change in the membrane potential that elicits an action potential, this relationship, commonly known as the strength-duration relationship, defines the minimum current to be injected into a cell over a duration τ to elicit an action potential.

Modeling the ion channels as a voltage-independent current-source I_{pump}, as shown in figure 7(b) can be described by the following equation:

$$I_p = \begin{cases} I_{\mathrm{pump}} & \text{for } V > V_0 \\ 0 & \text{for } V = V_0 \\ -I_{\mathrm{pump}} & \text{for } V < V_0 \end{cases} \tag{9}$$

This system of equations leads to the derivation of the Weiss strength-duration relationship [105]:

$$I_{\mathrm{th}} = I_{\mathrm{rh}}\left(1 + \frac{\tau_{\mathrm{ch}}}{\tau}\right) \tag{10}$$

where $I_{\mathrm{rh}} = I_{\mathrm{pump}}$ and $\tau_{\mathrm{ch}} = \frac{C(V - V_0)}{I_{\mathrm{pump}}}$. In general, the Weiss model provides a better fit to experimental data than the

Lapicque model [2, 3]. More accurate descriptions of cellular activation need to take into account the voltage-dependent conductivity and dynamics of the ion channels, which can be described by the Hodkin–Huxley equations ([106], chapter 4).

3.2.2. Extracellular stimulation and the effect of pulse duration. Extracellular electrical stimulation is the mechanism by which all clinical neural implants operate today. It works by polarizing cells in an electric field, instead of directly injecting current into the cell. The cell membrane is highly resistive, while its cytoplasm is very conductive. Therefore, when an electric field is applied across a cell in the extracellular medium, charges redistribute along the cell membrane and the cytoplasm rapidly becomes equipotential (within tens of ns). As a result, the trans-membrane potential increases (i.e. the membrane becomes hyperpolarized) on the side of the cell facing the anode, and decreases (the membrane becomes depolarized) on the opposite side.

Changes in the trans-membrane voltage affect conductivity of the trans-membrane voltage-sensitive ion channels, which typically leads to an increased influx of cations (Sodium in ganglion cells, Calcium in bipolar cells) on the depolarized side of the membrane, resulting in cellular depolarization as a whole. This, in turn, leads to further opening of the sodium channels, which accelerates the charge intake. When the membrane potential exceeds a certain threshold, an action potential occurs in spiking neurons. Within about a ms, the action potential ends when the sodium channels are inactivated (closed) and the slower potassium channels open up, leading to an outflux of K^+ ions, which lowers the membrane potential back to its resting value. Ion pumps then restore normal ion concentrations within a few ms ([106], chapter 4).

Extracellular electrical stimulation only depolarizes the cathode-facing section of the cell membrane. Therefore, it can only recruit a small fraction of all the ion channels present on the cell membrane to elicit an action potential, and requires stronger stimuli to elicit responses than what uniform depolarization of the whole cell membrane would require. Typically, at least a few tens of mV must be applied across a cell soma to elicit a response, while a few mV can suffice for intracellular stimulation [12].

If an action potential occurs during the stimulation pulse, the threshold current does not depend on pulse duration. This regime of stimulation is called the rheobase (see figures 8(a) and (b) for examples). When the stimulus ends before the action potential is generated, the influx of sodium ions during the stimulus may still be sufficient to put the neuron on the path to generating an action potential. For this, the sodium influx during the stimulus should exceed the stimulation threshold. The shorter the pulse, the stronger the stimulus needs to be in order to open enough ion channels and allow sufficient charge influx to exceed the stimulation threshold. This mechanism defines the rising part of the strength-duration dependence of the stimulation threshold [12] with decreasing pulse duration. The kinetics of different ion channels can vary significantly, and therefore the strength-duration dependence of the stimulation threshold varies for different cell types [12].

For intracellular stimulation, the stimulation threshold can be approximated as the charge required to depolarize the cell by a certain voltage, and therefore the threshold current scales reciprocal to pulse duration in this regime. In extracellular stimulation, however, dynamics of the charge influx are more complex, and the strength-duration curve deviates from such a simple shape [12]. For round cell somas, polarization is driven by the electric field across the cell. In cell axons, it is instead driven by the derivative of the electric field along the axon ([106], chapter 21).

The strength-duration relationship is usually characterized by a time constant (the chronaxie) and its asymptotic value (the rheobase), which are obtained by fitting power functions or exponentials to the data. The chronaxie, a classical measure of responsiveness of a neuron, is defined as the duration at which the threshold current is twice the amplitude of the rheobase. Typically, the chronaxie in ganglion cells is shorter than in bipolar cells (figure 8), which provides an opportunity for selective stimulation of various cell types, as described in the next section.

3.2.3. Role of electrode placement and pulse polarity. Since the distribution of ion channels over neurons is rarely isotropic, orientation of the electric field significantly affects the stimulation threshold. It is lower when the side of the cell with the highest concentration of the responding ion channels (Na for ganglion cells, Ca for bipolar) is depolarized. Therefore, placement of the stimulating electrode (epiretinal or subretinal) as well as pulse polarity (anodic or cathodic) affects the stimulation thresholds.

Dependence of the stimulation threshold on pulse polarity has been confirmed many times experimentally. For epiretinal stimulation of RGCs, cathodic-first pulses have a lower stimulation threshold [11, 77, 107] due to the higher concentration of Na channels over the region of RGCs facing the inner limiting membrane, near the axonal hillock [107]. For subretinal stimulation of RGCs, anodic-first pulses have lower stimulation thresholds for the same reason [108]. Similarly, for subretinal stimulation of the inner nuclear layer, anodic pulses have a lower threshold [11, 109] because bipolar cells have a higher concentration of Ca ion channels towards the epiretinal side. Stimulation thresholds can be 2 to 7.5 times lower with anodic-first pulses than with the opposite polarity [11, 108]. For small electrodes, proximity to the target neuron is another factor that significantly affects the stimulation thresholds, since in this case the electric field rapidly decreases with distance. A combination of good electrode placement and proper choice of the stimulation pulse parameters can help achieve selective activation of the various retinal layers [11].

Generally, RGC responses to electrical stimulation can be classified into three categories, depending on their origin. Short Latency (<2 ms) RGC responses correspond to action potentials elicited directly in the ganglion cells. Medium Latency responses (typically on the order of 3–50 ms) are mediated by stimulation of the inner nuclear layer. Electrical stimulation of the photoreceptors accounts for long latency responses (figure 8) (>50 ms). Selectivity of stimulation quantifies the ability to activate one layer of cells without affecting the others, and is

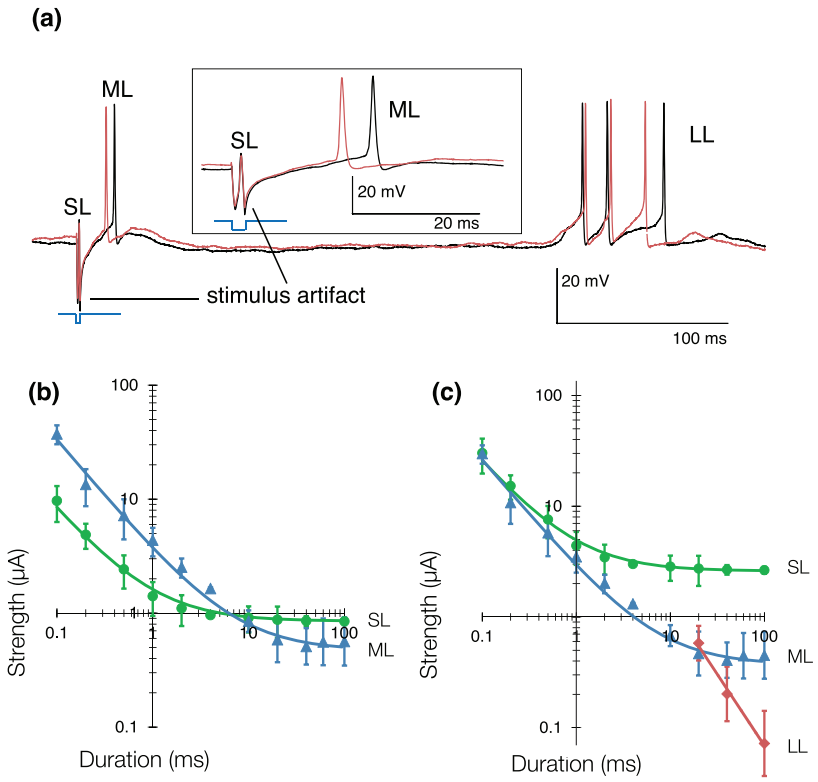

Figure 8. Selective subretinal activation of the retina. (a) RGCs respond to electric activation of the retina with a combination of short (SL), medium (ML) and long latency (LL) action potentials. SL responses come from direct activation of the RGCs, while ML responses originate in the inner nuclear layer, and LL responses likely originate in the photoreceptor layer. (b) Strength-duration relationship for a stimulating electrode placed epiretinally delivering cathodic-first current pulses. Short (<2 ms) pulses can selectively activate the RGCs, while long (>10 ms) pulses can selectively activate the INL. (c) Strength-duration relationship for a stimulating electrode placed in the outer plexiform layer (subretinal positioning) delivering anodic-first current pulses. Long (10 ms) anodic pulses can activate the INL without eliciting activity in the GCL. Data adapted from [11].

defined as the inverse ratio of the stimulation threshold of the layer of interest versus that of other layers.

Epiretinal prostheses aim at eliciting RGC responses through direct stimulation, so selectivity for this approach is the threshold for medium latency action potentials divided by the threshold for short latency action potentials. Measurements of the strength-duration relationships of direct and network-mediated responses [11] (figure 8) demonstrated that short (<1 ms) cathodic-first pulses coming from an epiretinal electrode with a distant return electrode provide a selectivity of 3 at best.

For subretinal prostheses, selectivity is the ratio of short latency action potential thresholds over medium latency action potential threshold, as subretinal implants generally target cells in the inner nuclear layer. Long (>4 ms) anodic-first pulses in the outer plexiform layer (i.e. in a subretinal position) provide the best selectivity, exceeding 6 for 20 ms pulses [11] delivered through an electrode with a distant return.

Relative positioning of the active and return electrodes in the implant affects the cross-talk between neighboring pixels, and thereby can also affect selectivity, contrast and attainable resolution [46, 51, 110]. Many implants operate with a common remote return electrode, in the so-called monopolar configuration. Cross-talk between neighboring pixels becomes more pronounced with a higher number of simultaneously activated pixels. To circumvent this limitation, arrays in which each stimulating electrode is surrounded by a local return electrode have been developed [46, 47]. A drawback of using local return electrodes is that they decrease the penetration depth of the electric field, compared to a monopolar configuration with the same pixel size, which imposes more stringent limits on the proximity between the stimulating electrodes and target cells. This has led to the development of 3 dimensional implants described in the following section.

3.2.4. 3 dimensional interfaces. The unexpected discovery that retinal tissue robustly migrates into voids in the subretinal space, even through small apertures, suggested the possibility of improving the contact between stimulating electrodes and target cells by making subretinal implants three dimensional, as opposed to planar implants [51].

Structures with chambers and pillars were found to induce retinal migration, with voids in the subretinal space being filled within days after implantation [55]. Cells in the inner nuclear layer easily migrate through apertures larger than 10 μm, while only cell processes migrate through smaller apertures. Similarly, cells migrate into the space between pillars (figure 9). With 10 μm-diameter pillars and 40 μm center-to-center

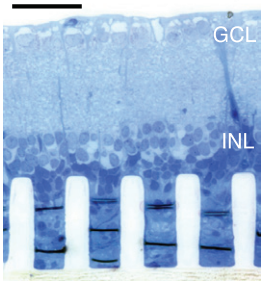

Figure 9. Retinal migration with pillar implants. The retina robustly migrates into the voids left by pillar implants in the subretinal space in a few weeks post-implantation. Cells in the inner nuclear layer (INL) reach close proximity with the top of the pillars. Pillars diameter: 20 μm. Spacing between pillar centers: 40 μm. Scale bar: 50 μm.

spacing, both cells of the inner nuclear layer and a substantial number of Müller cells fill the space between pillars. With 20 μm spacing between pillars, the space is filled mostly with Müller cell processes [55]. In general, pillar implants appear to maintain a more natural topology of the various retinal layers than implants with chambers, although it is unclear if this has implications for retinal prostheses or not.

Three dimensional interfaces are associated with two significant drawbacks: (1) fabrication is more difficult, and (2) integration of the retina into three dimensional structures precludes their explantation. Innovative microfabrication processes are being developed to circumvent the first limitation [111], but no data on active 3 dimensional implants has been published to date.

3.3. Retinal response to stimulation ex vivo

Epiretinal and subretinal implants share the common goal of encoding visual information in a degenerate retina. However, they rely on activation of two different neural layers to elicit visual percepts. While the epiretinal approach focuses on stimulating the ganglion cells, the subretinal approach aims at eliciting activity in the inner nuclear layer. As such, retinal response to epiretinal and subretinal stimulation differs greatly, and the encoding strategies for both types of implants should vary accordingly.

3.3.1. Epiretinal stimulation. Retinal ganglion cells are spiking neurons that encode visual information in the form of trains of action potentials. Therefore, epiretinal implants try to directly elicit trains of action potentials in the RGCs, with each stimulation pulse encoding a single spike. Responses of RGCs to direct activation with electrodes of various sizes have been studied extensively [59, 87, 112, 113]. Typically, RGCs respond to direct activation with a single action potential elicited within 3 ms of the stimulation pulse, and latency of the response decreases with increasing stimulus strength [11]. The good temporal precision of direct RGC activation makes it possible to envision multiplexed activation strategies, where only a few electrodes are activated at the same time. Multiplexed activation reduces cross-talk between neighboring electrodes, and might be beneficial for achieving higher spatial confinement of electric fields [110].

The probability of eliciting an action potential in a RGC increases with stimulus amplitude following a sigmoid function [114, 115], and stimulation thresholds in the literature usually correspond to a 50% probability of eliciting a response, although sometimes a 90% probability definition is used as well. As described in section 3.2, the amount of current required to elicit an action potential depends strongly on pulse width. A survey of available stimulation threshold data indicates that typically, charge density thresholds are in the range 0.1–1 mC cm^{-2} with stimulation pulses not exceeding 1 ms [113]. In some RGC subtypes, stimulation thresholds for direct activation can increase with retinal degeneration. RGC types for which stimulation thresholds do not change with degeneration exhibit abnormal spontaneous oscillations [90].

Studies with rabbit retina demonstrated that the region of minimum threshold for direct activation corresponds to the area of high-density sodium channels at the beginning of an axon in RGCs [115]. This is consistent with theoretical models of extracellular electrical stimulation, which predict that the intake of sodium on the depolarized side of the membrane is responsible for triggering the action potential.

RGCs can generally respond to stimulation pulses at frequencies of at least 100 Hz [113], which makes it possible to produce naturalistic trains of action potentials with electrical stimulation [116]. The maximum frequency at which RGCs can follow stimulation pulse trains depends on the cell type. For example, in the rabbit retina, brisk-transient cells can follow pulse trains at rates as high as 600 Hz for a full second, while local edge detectors and ON-OFF direction selective cells fail to follow pulse trains at 200 Hz for a 1 s-long stimulus [117]. In comparison, the amplitude of RGC responses to network-mediated stimulation decreases dramatically with increasing pulse frequency, and RGCs barely respond to individual stimuli above 10 Hz (see section 3.4.2).

Consequently, epiretinal implants that aim at restoring the natural visual code in each retinal ganglion cell [107, 116] should be able to activate individual RGCs without affecting the surrounding cells. Different ganglion cell types were found to have somewhat different activation thresholds in the rabbit retina [115], likely due to differences in sodium-channel bands and other anatomical or physiological properties. More complex shaping of the stimulation pulses might further improve stimulus selectivity to a given cell type.

Selective activation of single RGCs has also been attempted by shaping of the electric field with dense arrays of microelectrodes. Encouraging results have been reported in the peripheral primate retina, where half of the somas of midget cells, which are thought to subtend high-acuity vision, could be activated without affecting surrounding parasol and small bistratified cell somas [114]. It is not known, however, whether these pulses also affected the ~15 RGC types of the primate retina other than midget, parasol and SBCs in this study. It also remains unclear how well spatial activation strategies will work for the more central areas, where retinal ganglion cells stack up on top of one another, instead of forming a monolayer of cells, like in the periphery.

A major issue with epiretinal activation of RGCs is axonal stimulation [118]. Axons from distant cells are located in the nerve fiber layer, between the stimulating electrodes and the ganglion cells. Axonal and somatic stimulation thresholds are similar to somatic [119], and therefore epiretinal implants often activate not only the target RGCs, but also the axons of distant RGCs which pass close to the stimulating electrode, resulting in arcuate visual percepts. This effect, and the associated distortion of the retinotopic map, remains a major hurdle that epiretinal implants will need to overcome in order to provide meaningful visual percepts to blind patients.

A promising approach for circumventing the problem of axonal stimulation is based on the application of long stimulation pulses to activate the inner nuclear layer rather than the ganglion cells [118]. Doing so significantly improves the localization of phosphenes in patients, however, the limitations associated with network-mediated stimulation (see sections 3.3.2 and 3.4.2) are likely to apply with this scheme.

3.3.2. Subretinal stimulation. Subretinal implants aim at eliciting activity in the retinal ganglion cells by stimulating neurons in the inner nuclear layer. The hope is to leverage some of the signal-processing properties of the retinal network, and thereby creating action potential patterns in the RGCs that resemble those arising under normal physiological conditions. Network-mediated retinal stimulation can retain some features of natural retinal signal processing, such as flicker fusion, adaptation to static images and non-linear summation of subunits in RGC receptive fields, as described in section 3.4. However, indiscriminate concurrent activation of different cell types in the inner retina, most evidently the ON and OFF pathways, precludes accurate reproduction of the natural retinal code with subretinal implants.

A few nC of charge injection from subretinal electrodes are required to activate the inner nuclear layer using anodic-first pulses [108]. For a photovoltaic prosthesis, this translates into light intensity thresholds on the order of 1 mW mm^{-2} [47, 99, 109]. Thresholds depend on pixel size and on configuration of the return electrodes. For subretinal pixels of 70 μm in width (with 18 μm electrodes), the lowest stimulation thresholds reported to date have been 0.33 ± 0.05 mW mm^{-2} with 10 ms pulses, well below optical safety limits (see section 2.3.2).

The mechanisms mediating retinal response to subretinal stimulation are not as well understood as those for direct activation of RGCs. It has been hypothesized that activation of the bipolar cells is responsible for the bursts of action potentials that arise from network-mediated electrical activation [120], with a wide range of latencies and number of action potentials elicited per stimulation pulse [11, 77, 121]. The number of elicited spikes increases with stronger and longer stimuli [47, 122], which makes it possible to encode the strength of the retinal response by controlling pulse amplitude and duration (figure 10). Such dependence is consistent with increased activation of the excitatory bipolar cells in the retina using stronger stimuli. However, since the inner nuclear layer also contains amacrine cells, inhibitory pathways are also likely activated by subretinal stimulation.

As with natural vision, retinal response to network-mediated stimulation greatly diminishes with increasing activation frequency, dropping close to zero (<10%) at 20 Hz *ex vivo* [49, 123] and at about 40 Hz *in vivo* [49, 99] (figures 11(a) and (b)). Healthy retinas respond faster to subretinal stimulation than degenerate ones [109]. This decrease in amplitude of the retinal response has been described both as 'desensitization' [120] of the retina, as well as more recently 'adaptation' to constant stimulation [49]. With natural vision, adaptation to high frequency stimulation is responsible for a continuous perception under stroboscopic illumination, such as CRT or DMD displays.

Adaptation to repeated electrical stimulation [49, 120] has been observed in both ON and OFF RGCs. Its extent varies greatly between cells, but it is still unknown whether various cell types have different characteristic patterns of adaptation to repeated electrical stimulation. While for some cells responses to individual pulses are gone at frequencies as low as 4 Hz, other do not adapt even at 40 Hz. The mechanisms causing adaptation to electrical stimulation are poorly understood. Pharmacological studies have showed that adaptation to repeated stimulation remains in the absence of inhibitory input from amacrine cells [120], which indicates at a mechanism independent of the amacrine pathway. Repeated subretinal stimulation also does not significantly affect the thresholds for direct RGC activation [120], which indicates that adaptation occurs prior to the action potential generation mechanism in RGCs.

Unlike natural responses to pulsed light, subretinal electrical stimulation of a retina devoid of photoreceptors elicits only ON responses [124]. The lack of OFF responses is most likely due to indiscriminate concurrent depolarization of ON and OFF bipolar cells at the onset of stimulation pulses. The trains of action potentials elicited in a population of RGCs by a subretinal implant are therefore very different from natural vision, and proper interpretation of these signals as meaningful visual percepts relies on brain plasticity and learning of this new 'prosthetic retinal language'.

3.4. Characterization of prosthetic visual functions

Vision is commonly quantified by resolution, contrast sensitivity and dynamic range, and these properties have been studied extensively with retinal implants [49, 119, 124]. Another important feature is the perception of motion, which is thought to be transmitted by the parasol retinal ganglion cells in the primate visual system [22, 125]. Accuracy of representation of motion signals with retinal prostheses has, so far, only been explored with epiretinal implants, for which promising results were reported with the elicitation of naturalistic motion stimuli in the peripheral primate retina [116], even though this study did not address the possibility of unwanted axon activation.

One way to characterize prosthetic visual function is through *ex vivo* studies using multielectrode array recording techniques [47, 49, 114, 116, 124]. In those, a piece of retina is excised and pressed against recording electrodes. For the study of epiretinal stimulation, these electrodes can

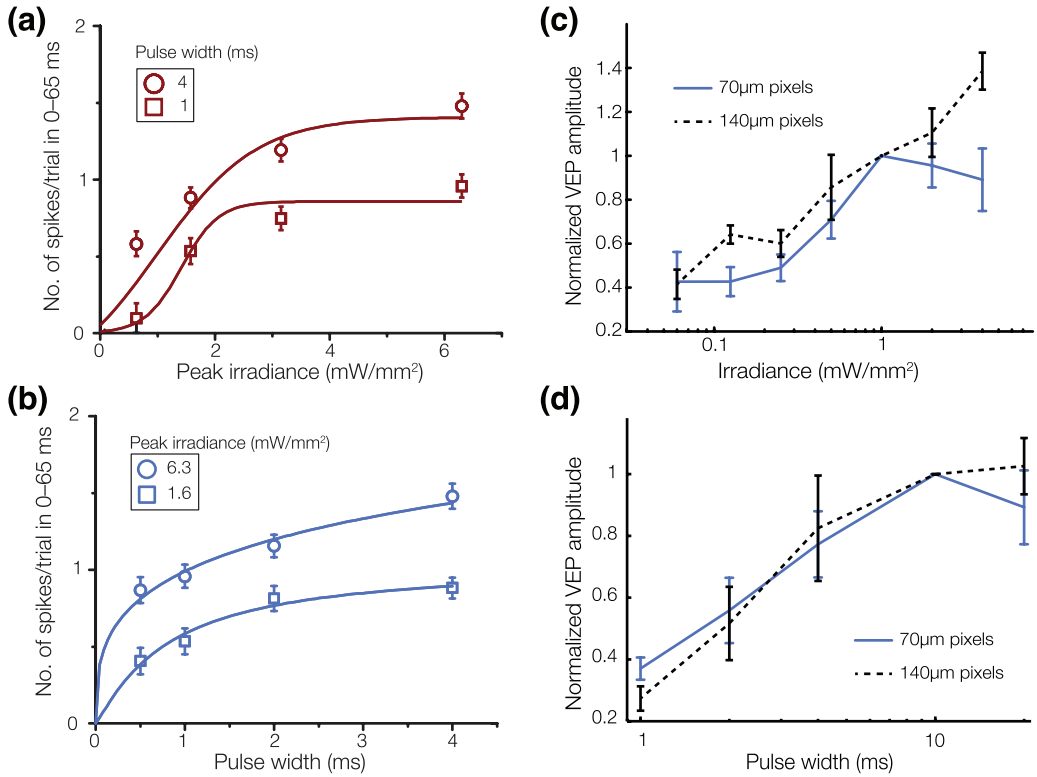

Figure 10. Modulation of RGC and cortical responses by pulse width and irradiance. At the level of the RGCs, the number of elicited action potentials increases with irradiance (a) and with pulse width (b). Error bars, s.e.m. At the cortical level, (c) devices with 70 μm pixels (blue) elicit a VEP response at 0.25 mW mm^{-2}, which increases up to 1 mW mm^{-2} and saturates beyond that level. The 140 μm pixels (black) have lower thresholds and do not saturate at high irradiance. (d) VEP amplitude increases with pulse duration between 1 and 10 ms, and saturates with longer pulses (with 2 and 4 mW mm^{-2} irradiance for 140 μm and 70 μm pixel devices, respectively). Error bars, s.d. Data adapted from [47, 109].

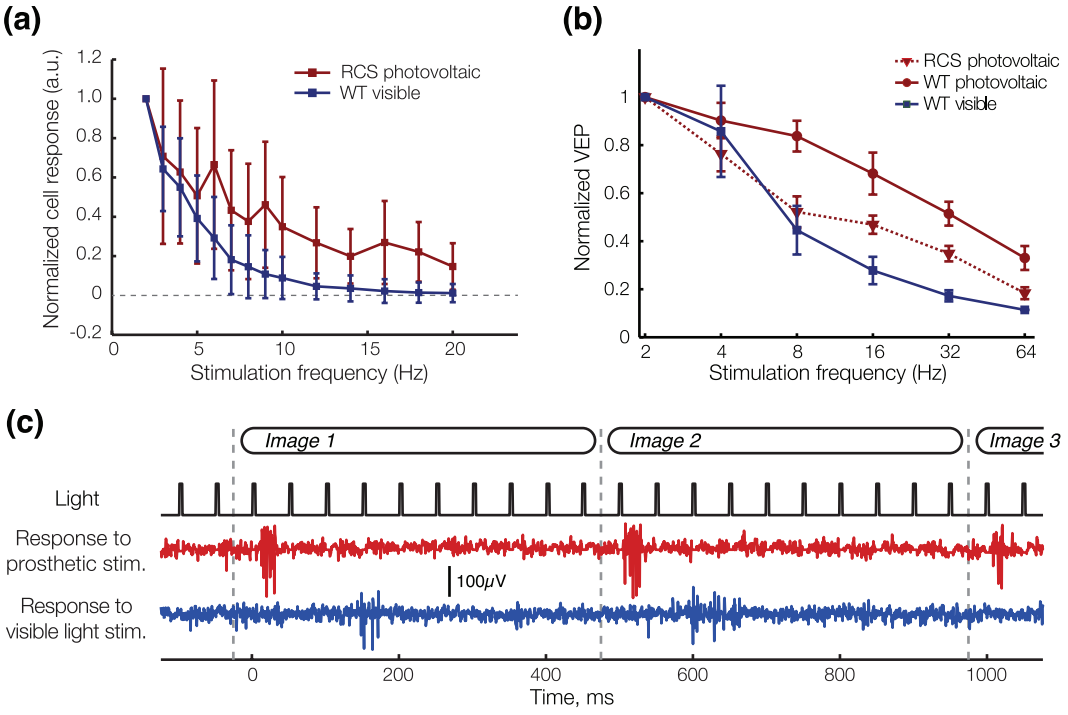

Figure 11. RGC and cortical adaptation to high frequency stimulation. (a) Average steady-state response of RGCs to pulsed stimulation of varying frequency in arbitrary units (a.u.). Error bards, s.d. (b) Normalized amplitude of the VEP response to visible (WT rats) and NIR (RCS rats) stimulation pulses of increasing frequency. Error bars, s.d. (c) With 20 Hz stimulation repetition rate, RGCs respond transiently to image changes and not to every pulse of electrical current (RCS) or visible light (WT), as illustrated in the single channel voltage recordings shown here. Grey dashed lines indicate the image refresh times. Adapted with permission from [49], copyright 2015 Nature.

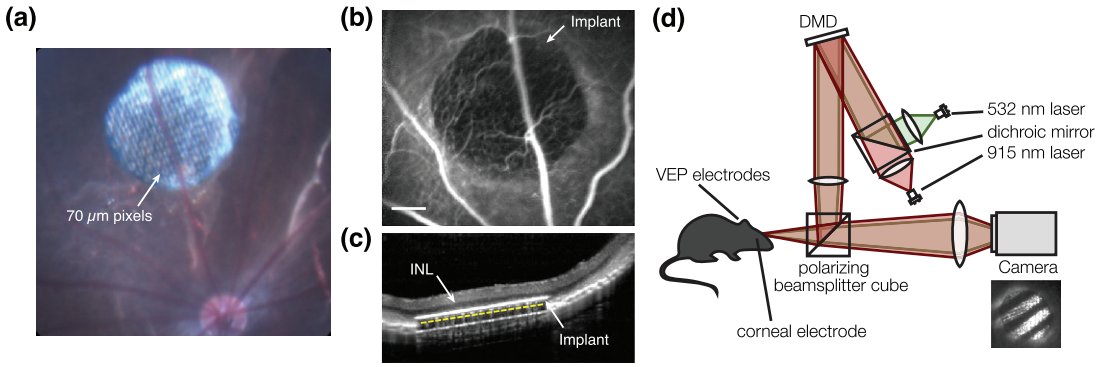

Figure 12. *In vivo* evaluation of an implant. (a) Fundus image of a subretinal photovoltaiv prosthesis with 70 μm pixels implanted in a rat eye. (b) Fluorescein angiography of a different RCS retina 1 week after implantation demonstrates normal retinal blood perfusion above the implant with no leakage. The implant is opaque to visible light and masks the choroidal fluorescence in the implanted area. Scale bar, 200 μm. (c) In an implanted RCS retina, OCT shows good preservation of the inner retina, with the inner nuclear layer (INL) located $\sim$20 μm above the upper surface of the implant (white line). The implant (30 μm in thickness) appears thicker than it actually is because of its high refractive index. The yellow dashed line illustrates the actual position of the backside of the implant, which is located on top of the retinal pigment epithelium. Horizontal and vertical scale bars, 200 μm each. (d) The *in vivo* stimulation and recording system consists of a visible (532 nm) and a NIR (915 nm) laser, which illuminate a digital micromirror device (DMD). In turn, this device generates the images projected onto the retina, as shown in the photograph (inset). Projected patterns are monitored by means of a CCD camera. Adapted with permission from [49], copyright 2015 Nature.

also deliver current pulses. For subretinal studies, an array of stimulating electrodes is put in contact with the photoreceptor side of the retina.

For *in vivo* characterization, studies begin with implantation of the prosthesis in an adequate animal model. For example, a subretinal photovoltaic prosthesis can be implanted in a rat [99]. Surgery begins with a trans-scleral incision, followed by the creation of a retinal detachment using saline solution [49, 99]. The implant is then slid into the opening, which is subsequently sutured. Integration of the device into the subretinal space can be evaluated by optical coherence tomography (OCT) and fluorescein angiography (figure 12).

For evaluation of prosthetic vision *in vivo*, cortical signals called Visually Evoked Potentials can be measured via chronically implanted trans-cranial electrodes placed over the visual cortex [126] (figure 12). In addition, corneal measurements of the waveforms produced by the implant can help evaluate charge injection by individual pixels, and follow them over the lifetime of the animal [109].

3.4.1. Resolution. One of the most important characteristics of vision in general, and in prosthetic restoration of sight in particular, is visual acuity. Since epiretinal and subretinal implants target different layers of the retina, the means by which resolution of epiretinal and subretinal implants are assessed *ex vivo* also vary.

Assessing resolution with an epiretinal implant ex vivo Epiretinal stimulation directly activates RGCs, and spatial resolution in this approach is linked to the number of ganglion cells an epiretinal implant can address independently. To restore normal visual acuity, it would likely need to address independently all of the patient's OFF midget RGCs in the central areas of the retina, as this cell type is thought to mediate high-acuity vision in primates [127]. Addressing RGCs independently of their neighbors offers the opportunity of encoding visual information specific to the cell type, such as motion signals in peripheral parasol RGCs, for example [116].

The best *ex vivo* results reported to date in the primate retina correspond to selective activation of approximately half of the OFF midgets over a 1 mm^2 area, without interactions with neighboring parasol or midget cells [114], using a 60 μm pitch epiretinal array. The experiment was conducted at eccentricities 35°–75°, where visual acuity is on the order of 20/400. Other RGC types were ignored in this study, and further work should evaluate how they respond to electrical stimulation.

RGCs are traditionally classified functionally on the basis of their light response properties [83]. This method cannot work in a degenerate retina that has lost its photoreceptors. Instead, cell classification methods based on electrical signatures of the RGCs, called their electrophysiological images [128], have been proposed [129], and enable cell classification without any light response properties (figure 13). These methods have yet to be demonstrated in a degenerate retina.

Assessing resolution with a subretinal implant Subretinal stimulation elicits RGC responses indirectly, via activation of the neurons in the inner nuclear layer. Consequently, the responses elicited in RGCs are shaped by the synaptic connections in the receptive field of the various ganglion cells.

Anatomical studies have shown that the receptive fields of midget cells in the primate fovea are relatively straightforward: a single photoreceptor connects to a single bipolar cell, which in turn connects to a single retinal ganglion cell [130]. Therefore the sampling density of the photoreceptors mosaic limits visual acuity in the fovea [127]. To restore normal visual acuity, one would need to stimulate individual bipolar cells in the fovea independently, much like an epiretinal implant would need to address individual ganglion cells. As functional recording of the primate fovea have yet to be achieved, pre-clinical studies of subretinal prostheses are conducted on RGCs that have more complex receptive fields, and for which the mechanisms that lead to high visual acuity are less well understood.

RGC receptive fields provide a description of the spatial extent of the visual field sampled by individual retinal

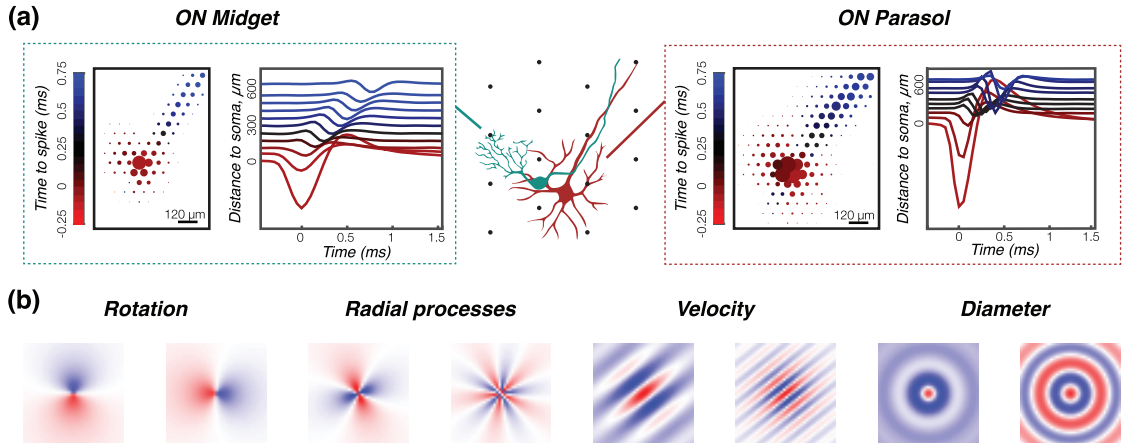

Figure 13. Classifying retinal ganglion cells without visible light information. (a) Multielectrode arrays record a 2D projection of spatio-temporal action potentials, called electrophysiological images (EIs), and schematically illustrated here for a midget (left) and a parasol (right) RGC. Differences in cell morphology lead to differences in the EIs. (b) Examples of handcrafted filters that can extract discriminative features of EIs, such as amount of rotation, number of radial processes, diameter, velocity of propagation of the axonal action potential in the EI. Classifiers can be trained to recognize cell types using these features. Adapted with permission from [129].

ganglion cells. Measuring them with prosthetic stimulation in essence characterizes the combined point spread function of the implant and the retinal network [109, 131]. A recent study demonstrated that with a subretinal array with 70 μm-wide pixels, the electric receptive fields in the degenerate rat retina are comparable in size to the natural receptive fields in a healthy rat retina (203 ± 63 μm versus 244 ± 32 μm).

The visual acuity of normally-sighted rats evaluated through behavioral measurements is approximately 1 cycle per degree [132], which corresponds to a much higher spatial resolution (30 μm on the retina) than the average size of receptive fields reported in the literature [49]. A possible explanation for this discrepancy is that RGCs also respond to movements of fine structures over their receptive fields [133–135] thanks to nonlinear spatial integration of bipolar cell sub-units that connect to the same ganglion cell [136–139]. The hallmark of nonlinear spatial integration in a receptive field is a frequency doubling in the RGC response to alternating gratings presented over the extent of the receptive field [140]. Linear summation of the bipolar cells output in the RGC should lead to a constant ganglion cell output as the contrast of a fine grating is alternated over the extent of the receptive field. However, a number of mechanisms can lead to nonlinear interactions between bipolar subunits [141], which in turn causes modulation of the RGC output when a fine texture moves over its receptive field (figure 14). Extracting spatial location information from non-linear subunit interactions in the receptive fields of RGCs would require a population-level decoding of the retinal signal by the brain.

Such nonlinear interactions with a subretinal prosthesis have been measured using alternating gratings projected over a subretinal photovoltaic array with a pixel pitch of 65 μm [49], and the results were compared to the response of the healthy retina to similar stimuli. The experiments were conducted with 20 Hz stimulus repetition rate and 1 Hz grating alternation. In healthy retina, very little, if any response to individual pulses of visible light were observed at 20 Hz, while RGCs responded strongly to the grating contrast

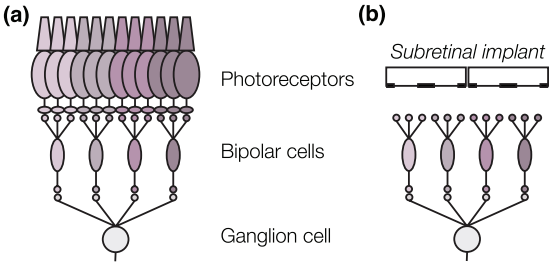

Figure 14. Nonlinear subunits in a receptive field. (a) The receptive field of a RGC can be broken into subunits that correspond to the receptive fields of each bipolar cell connecting to the RGC. (b) A subretinal prosthesis with small enough pixels can activate independent subunits, which then sum up nonlinearly in the retinal ganglion cell.

reversal (figures 11(c), 15). Electrical stimulation resulted in a continuum of responses, ranging from a combination of very weak responses to individual pulses at 20 Hz and strong transient responses to the alternating grating, to more robust responses to every stimulation pulse. Neurons responded to electrical grating alternation with stripes down to 68 μm, and with visible light to 28 μm stripes (figure 15). RGC responses to the alternation of gratings smaller than their receptive fields showed evidence of frequency doubling, which indicates nonlinear subunit interactions. It also demonstrates that electrical stimulation can be spatially localized to subunits of the RGC receptive fields, and the width of the subunits matches the pixel pitch.

Alternating gratings are also a well-established method for assessing visual acuity in animals and in human infants, which is carried out in practice by recording visually evoked potentials (VEPs). With normal vision, this method matches well the visual acuity measured in behavioral tests [142, 143]. For prosthetic vision in RCS rats implanted with photovoltaic arrays having 65 μm pixel pitch, the spatial resolution measured from visually evoked potentials was 64 ± 11 μm per stripe, as compared to 27 ± 9 μm per stripe in WT animals stimulated with visible light (figure 15(c)). These values correspond to 0.47 and 1.1 cycles per degree (cpd) respectively,

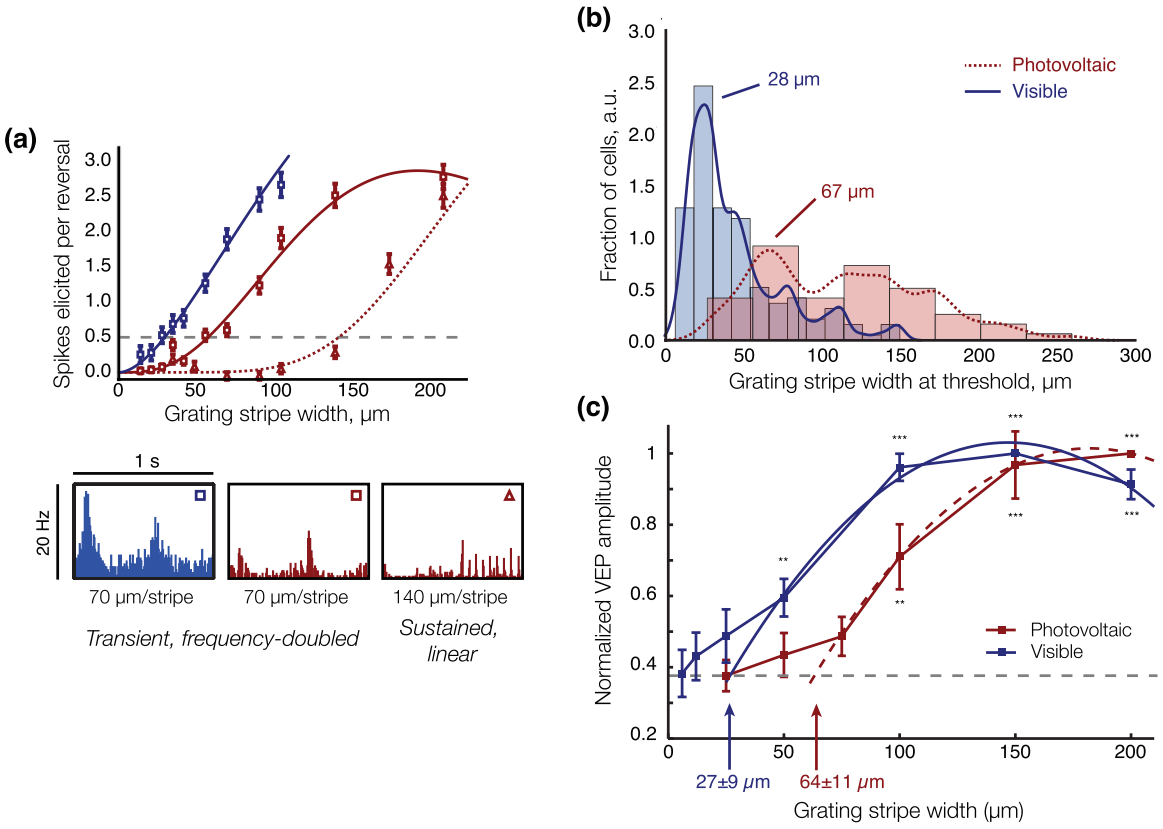

Figure 15. Response to alternating gratings. (a) Amplitude of the response to grating reversal as a function of the grating stripe width, for one sample neuron stimulated with visible light (blue, WT retina) and two sample neurons stimulated with a subretinal photovoltaic prosthesis (red, RCS retina, triangles and squares). Stimuli were displayed with 20 Hz, 4 ms pulses stroboscopic illumination and 1 Hz grating contrast reversal period. The dashed gray line indicates the stimulation threshold. Peristimulus time histograms show the response of the neurons for alternation of 70 μm-wide gratings. The WT response exhibits frequency doubling, indicative of non-linear interactions in receptive field subunits. Prosthetic responses range from flicker-fused and frequency-doubled (left histogram), to more sustained and linear (right histogram). Error bars, s.e.m. (b) Histograms and kernel density estimates of the stimulation thresholds distributions (0.5 action potential/reversal). The peak in the distribution occurs at 28 μm for visible light stimulation. With photovoltaic stimulation, a first peak occurs at 67 μm. (c) Normalized VEP amplitude for visible gratings (blue) and photovoltaic (prosthetic) stimulation (red) measured as a function of grating stripe widths. The acuity limit, estimated as the crossing point of the parabolic fits with the noise level (dashed lines), corresponds to 27 ± 9 μm/stripe for visible light and 64 ± 11 μm/stripe for prosthetic stimulation. Error bars, s.e.m. NS, not significant; $^{*}P < 0.05$; $^{**}P < 0.01$; $^{***}P < 0.001$, one-tailed Welch t-test performed against the lowest grating size group. Adapted with permission from [49], copyright 2015 Nature.

in close agreement with the visual acuity of pigmented rats reported in the literature [132]. In a human eye, 65 μm pitch geometrically corresponds to a spatial resolution on the retina as expected with 20/250 visual acuity.

3.4.2. Dynamic range and contrast sensitivity. If one could elicit naturalistic spike trains in all types of RGCs with epiretinal stimulation, it would be possible to encode the full dynamic range of natural vision. However, RGC hyperactivity in degenerate retina and the lack of selective activation of various types of RGCs currently preclude this possibility.

With low-frequency (2 Hz) activation of a subretinal implant, the number of elicited spikes in RGCs can be modulated by pulse width and amplitude [47] (figures 10 (a) and (b)). Likewise, amplitude of the cortical signals can be modulated by stimulus width and amplitude, over approximately an order of magnitude [99, 109] (figures 10 (c) and (d)). With high-frequency flicker-fused stimulation, the full-field contrast sensitivity of prosthetic vision is 10 times lower, and the dynamic range is two times below that of natural vision [109, 124]. To elicit robust responses in the RGCs or in the cortex, a photovoltaic subretinal prosthesis requires positive contrast steps larger than 50% in Michelson units, compared to only a few percent required with normal vision. In addition, negative contrast steps do not elicit responses in degenerate retina with prosthetic stimulation (figure 16).

The implications of reduced contrast sensitivity on efficiency of delivery of visual information have only recently begun to be explored [124]. During visual fixation on a static scene, the retina locally adapts to the average luminance over the course of a few hundred milliseconds [144]. RGCs then respond to local changes in contrast triggered by a range of ocular movements, such as microsaccades, drift and ocular tremor. Recent studies [145] have shown that the statistical properties of fixational eye movements (FEMs) are well tuned to the statistics of natural scenes, and perform whitening of spatial frequencies below 30 cycles per degree—the resolution limit of a typical human eye. Contrast sensitivities of RGCs are, in turn, well adapted to the resulting spatio-temporal patterns of light on the retina, producing robust RGC responses. The significantly lowered contrast sensitivity of prosthetic vision is likely to disrupt these finely tuned fixational mechanisms, as recent models have suggested [124].

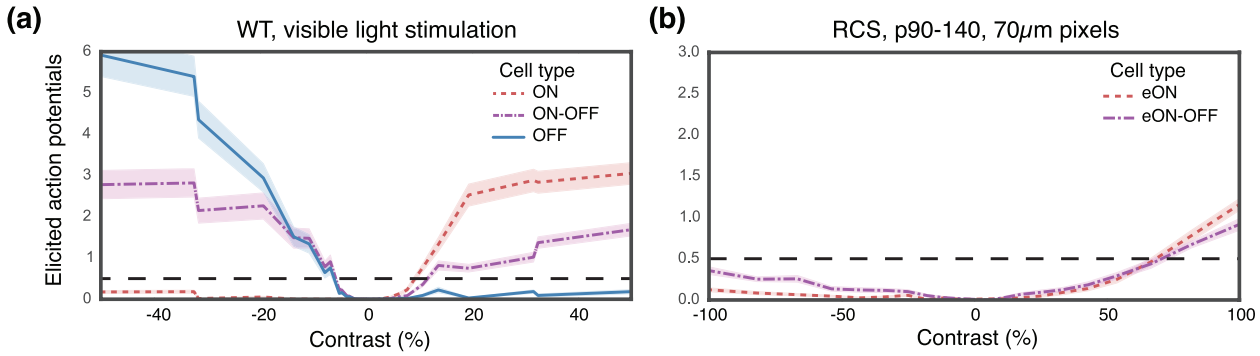

Figure 16. Mean population responses of RGCs to full-field subretinal contrast steps. (a) WT responses to visible full field light steps can broadly be classified into vON (red), vOFF (blue) and vON-OFF (purple) responses. The black dashed line outlines the stimulation threshold, defined as a 50% probability of eliciting an action potential correlated with the contrast step. On average, ON cells respond to contrast increments greater than 7%, while OFF cells respond to contrast decrements as small as 3%. (b) Photovoltaic stimulation of p90-140 RCS retina with 70 μm pixel implants requires 67% contrast steps to elicit responses in the RGCs. Maximum amplitude of the response is lower than with visible light in the WT retina. Confidence bands represent the standard error of the mean. Adapted with permission from [124], copyright 2015 Association for Research in Vision and Ophthalmology.

These findings could explain the fading effects reported by patients with subretinal implants (see section 4.3), when fixating visual scenes. Empirically, these patients prefer low stimulation frequencies, in which high temporal contrast would compensate for the lack of contrast sensitivity of prosthetic vision. Image processing involving contrast enhancement and image sparsity might improve their performance.

4. Clinical results

The ultimate assessment of prosthetic vision is conducted by careful psychophysical evaluation of the visual percepts elicited in patients. A number of groups have reached this stage, thereby providing invaluable evidence that implants can elicit meaningful percepts in patients suffering from severe retinal degenerations. In this section, we review the current status and results of the clinical studies of various prosthetic devices.

4.1. Standards for evaluating the performance of a retinal implant

The FDA has issued non-binding recommendations on how to perform assessment of visual function in their investigational device exemption (IDE) guidance for retinal prostheses [146]. A set of low vision tests called FLORA (functional low-vision observer rated assessment) was also recently introduced through the trial conducted by Second Sight Medical Implants (Sylmar, CA) of their Argus II retinal prosthesis [147]. The tests suggested by the FDA include the following: (1) low vision letter acuity with limited response time; (2) grating acuity using a forced-choice paradigm and fixed presentation time; (3) mapping of stimulated visual phosphene fields, including two-point discrimination tests; (4) assessment of form vision and functional vision in real-world situations, including orientation and mobility.

Other clinical trials [35, 37] have reported on static light perception, and often describe the perceived brightness, shape and color of those phosphenes. In addition to measurements of grating visual acuity, some patients could distinguish Landolt C-rings and read letters. Temporal characteristics of prosthetic vision and detection of motion are also frequently assessed.

4.2. The Argus II epiretinal implant

The only retinal prosthesis currently approved for commercial use by the FDA (as a humanitarian use device) is the Argus II epiretinal prosthetic system (Second Sight Medical Products, Sylmar, California, USA). It consists of a head-mounted unit, which includes a camera and an RF antenna that transmits the processed data to the intraocular implant by serial telemetry (figure 17). The inductively-delivered signals are decoded and processed inside the implant, before being distributed over 60 stimulating electrodes via a trans-scleral cable [148].

The array of stimulating electrodes is attached to the epiretinal surface with a trans-retinal tack [34]. The Argus II has now been implanted in over 100 patients, with a best reported grating visual acuity of 20/1260 [147, 149]. A number of serious adverse events (SAEs) affecting approximately 30% of the patients were reported over the course of the clinical trial [34], the majority (82%) of which occurred within the first 6 months. Conjunctival erosion and dehiscence over the extraocular implant were the most common occurrences [34, 149]. No device failures were reported within 3 years after implantation [147]. One year post-implantation, 20% of patients reported a neutral and 80% a positive outcome, while 3 years post-implantation, 35% of patients were neutral and the remainder remained positive about implantation. No negative opinion of the implant was reported.

All subjects in the Argus II clinical trial were able to perceive light with the implant turned on, and almost all but one subjects performed better at square localization with the implant than without it. Only 57% of subjects performing better at detecting the direction of motion with the system ON than OFF. The clinical trial also reported improved orientation and mobility with the system, but other studies have reported the opposite, with a statistically significantly

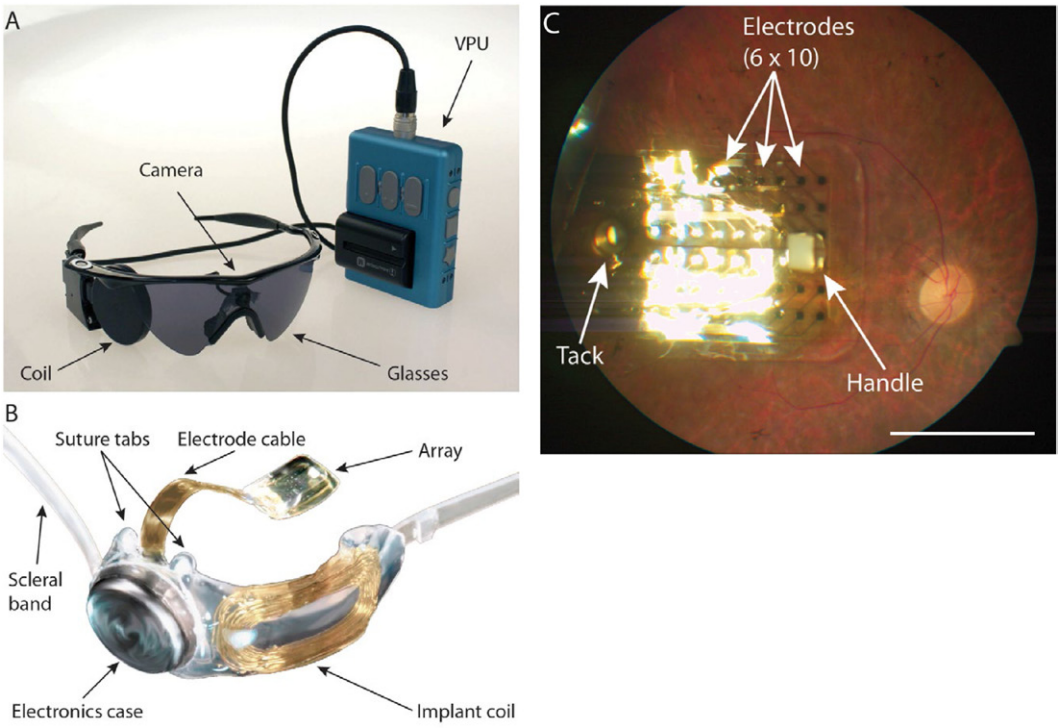

Figure 17. The Argus II epiretinal implant. (a) Photograph of the external portion of the Argus II prosthesis system (Second Sight Medical Products, Inc., Sylmar, CA) including glasses-mounted video camera, radio-frequency (RF) coil, and video processing unit (VPU) with rechargeable battery. (b) Photograph of the implanted portion of Argus II prosthesis system including the 610 electrode array, electronics case, and implant RF coil. (c) Fundus photograph of an Argus II array implanted in the macular region. A retinal tack secures the electrode array to the retina. The surgeon uses the white handle to position the device in the eye. Scale bar: 5 mm, corresponding to 16.7° visual angle. Adapted with permission from Humayun *et al* [34], copyright 2012 Elsevier.

worsened performance at spatial orientation tasks with the implant turned on [150]. One reason the Argus II implant could degrade spatial orientation could be the fact that the visual percepts it delivers are unrelated to direction of gaze. If it were indeed the reason, the addition of eye tracking and the corresponding image translation in the system would alleviate this limitation. Alternatively, it could be that the low-resolution visual percepts interfere with patient's natural orientation habits, including sounds and touch.

A significant limitation of the Argus II implant is the stimulation of axons passing between the stimulating electrodes and the ganglion cells. As a result, percepts have arcuate instead of punctate shapes [119, 151], which severely distorts retinotopic mapping of the visual field. The most promising solution to this problem currently is based on application of longer pulses (20 ms sinusoids instead of the typical 0.5 ms) to stimulate bipolar rather than ganglion cells, thereby invoking network-mediated retinal responses without axonal activation [118].

4.3. The Alpha IMS subretinal implant

The subretinal approach has been spearheaded in Germany by Retina Implant AG (Reutlingen, Germany) with their Alpha-IMS system [7, 35, 152], which received CE marking in 2013. In this device, a subretinal camera (a CMOS chip consisting of photodiodes and amplifiers) can transduce images naturally projected onto the retina with ambient illumination into electrical currents that stimulate neurons in the inner nuclear layer (figure 18).

The implant consists of 1500 72×72 μm^2 pixels made up of a 30×15 μm^2 photodiode and a 50×50 μm^2 Titanium Nitride electrode. The return electrode is common to all the pixels in the implant, and is located far from the stimulating electrodes. Power is delivered to the implant via a cable that runs underneath the retina through the sclera, and then under the skin, to a place behind the ear, where it is transferred inductively to the receiver with an RF transmitter (figure 18), like in cochlear implants.

Functional outcomes with foveal placement of the implant (eight patients) were significantly better than with parafoveal placement (12 patients) [152]. No patients with nonfoveal placement could distinguish direction of motion, while 75% of the patients with foveal placement managed to accomplish this task [35]. In another report including eight patients, all perceived light, 7/8 could localize the phosphenes and 5/8 perceived motion. One patient achieved a best Landolt C-ring visual acuity of approximately 50/550 [35]. The rest of the patients achieved equivalent visual acuities below 20/1000. Some patients managed to identify and count objects, and read large fonts (3/8). Patients preferred stimulation frequencies ranging from 1 to 15 Hz. No quantitative evaluation of the impact of the Alpha IMS prosthesis on mobility has been reported to date.

A recent study reported that without stimulation, the eye movements of RP patients implanted with the Alpha IMS

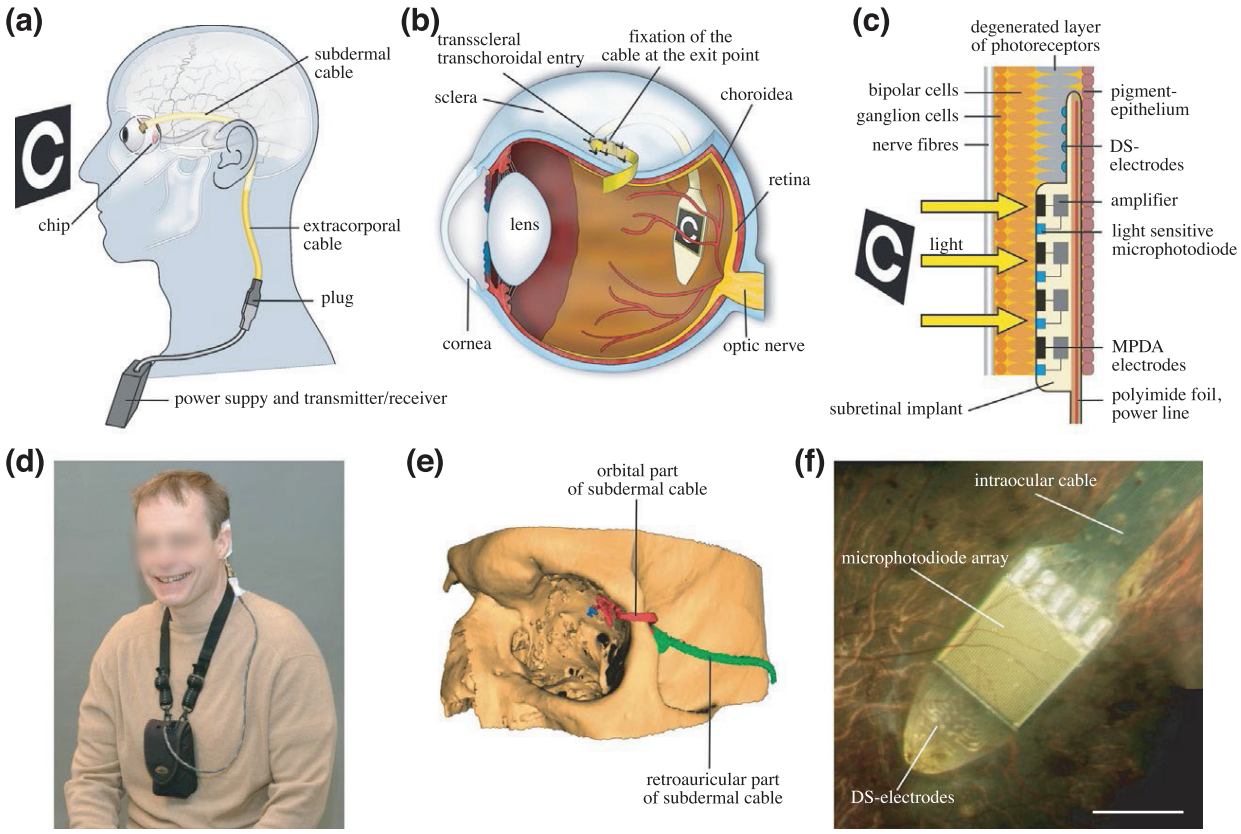

Figure 18. The Alpha IMS subretinal implant. (a) The cable from the implanted chip in the eye leads under the temporal muscle to the exit behind the ear, and connects with a wirelessly operated power control unit. (b) Position of the implant under the transparent retina. (c) MPDA photodiodes, amplifiers and electrodes in relation to retinal neurons and pigment epithelium. (d) Patient with wireless control unit attached to a neckband. (e) Route of the polyimide foil (red) and cable (green) in the orbit in a three dimensional reconstruction of CT scans. (f) Subretinal implant at the posterior pole photographed through a patient's pupil. Scale bar: 3 mm, corresponding to 10° visual angle. Reprinted from Zrenner *et al* [7] under the Creative Commons Attribution License, CC BY 4.0.

implant are large and scanning. With the implant ON, patients fixated well and direction of gaze corresponded to the stimulus location. They exhibited classic fixational eye movement patterns, including ocular tremor, drift and microsaccades. After stimuli disappeared, eye movements became large and scanning again [153].

4.4. Other clinical systems

A suprachoroidal approach to restoration of sight has been pursued by Bionic Vision Australia (three patients) [37], and Osaka University (2 patients) [154]. Phosphene perception remained over the 12 months Bionic Vision trial, but the equivalent visual acuity ranged from 20/4000 to 20/20000—well into the realm of ultra-low vision.

Clinical trials of the IRIS epiretinal implant have been conducted by IMI Intelligent Medical Implants AG. Since 2012, IMI operates as a subsidiary of Pixium Vision SA, which is continuing these trials. No reports on their functional outcomes have been made available to date.

Optobionics conducted a clinical trial of their Artificial Silicon Retina (ASR) implant, which was a passive subretinal array of photodiodes [50]. They reported improvements of central vision following implantation of the ASR in the periphery, possibly due to neurotrophic effects [155]. The company closed in 2007, and trials did not continue. The EPIRET3 system [45] was implanted in six patients for a period of 4 weeks and successfully elicited visual percepts; however, no long-term study of the implant has been conducted to date.

5. Other approaches to restoration of sight

5.1. Non-retinal electrical prostheses

Non-retinal electrical prosthetics may be used for treatment of the same diseases that retinal prostheses address, but also hold promise for conditions where ganglion cells are damaged, such as with glaucoma, or when the whole retina is missing, as in the case of trauma. In this section, we describe some approaches to non-retinal electrical restoration of sight.

5.1.1. Optic nerve stimulation. Two approaches to visual prostheses targeting the optic nerve have been explored. In one system, 4 electrodes are placed in a cuff around the optic nerve, delivering 0.1 ms bi-phasic charge-balanced pulses at frequencies varying from 50 to 333 Hz [156]. These electrodes elicited clusters of phosphenes, ranging in size from 8 to 42 min of arc. Their position in the visual field was within ±30 degrees, and depended on which of the four electrodes was activated. Spatial localization of the phosphenes shifted with changes in the

direction of gaze, as with the Argus II retinal prosthesis (see section 4.2). Development of this system has been abandoned, in part due to difficulties with encoding predictable visual patterns.

Another approach is based on an array of electrodes penetrating the optic nerve [157]. This approach offers a much larger number of electrodes, but it is much more invasive. With over 1 million axons tightly packed in the optic nerve, the major challenge of both approaches lies in achieving spatially selective stimulation. Stimulation of the optic nerve is unlikely to expand the range of clinical indications compared to retinal prostheses since if the ganglion cells are missing, their axons also degenerate.

5.1.2. Targeting the LGN. Retinal ganglion cells project to the dorsal lateral geniculate nucleus (LGN), which has been suggested as a potential target for electrical stimulation [158], especially for patients who lost their retinal ganglion cells due to glaucoma or ocular trauma. The relatively simple structure of the receptive fields in the LGN, compared to the visual cortex [159], and the over-representation of the foveal and parafoveal areas that mediate high acuity vision, compared to the retina, potentially simplify targeting the areas that represent central vision. To some degree, the LGN also has macroscopic segregation between the parvocellular pathway, which is thought to encode fine visual information and the magnocellular pathway, which relays motion signals to the brain. Such segregation could simplify the encoding of prosthetic visual information.

Electrical stimulation of the LGN elicited localized visual percepts in alert monkeys [158], which caused saccades to electrical targets comparable to normal visual saccades. However, this approach has not progressed very far, partially because of its very invasive nature.

5.1.3. Cortical visual prostheses. The best-known cortical visual prosthesis was developed by William Dobelle and dates back to the 1970s, with a first implantation in a patient in 1978, although other researchers had previously experimented with electrical stimulation of the visual cortex [160]. Activation of an electrode in the visual cortex often results in perception of a single spot of light color (bluish or yellowish), and its position in the visual field depends on location of the electrode and on the direction of gaze. Sometimes electrodes can elicit more complex phosphenes, composed of several spots [160], and even dark percepts. The Dobelle cortical implant failed to elicit useful visual percepts in patients and led to significant complications. In particular, electrical activation of the implant tended to be painful and sometimes triggered seizures [43].

Research on cortical visual prostheses continues [161], and Second Sight is adapting its retinal system to cortical implantation. However, this system is unlikely to provide high resolution vision in the near future due to the very low number of electrodes and our limited understanding of encoding of visual information in the brain.

5.2. Optical stimulation

Many optical approaches to restoration of sight are also being explored as an alternative to electrical stimulation.

5.2.1. Optogenetics. Optogenetic approaches to restoration of sight are based on the transfection of neurons by a viral vector, which causes these cells to express a light-sensitive ion channel based on opsin molecule [162]. Cation channels, such as channelrhodopsin, and anion pumps, such as halorhodopsin, enable excitatory and inhibitory optical control of neural activity, respectively.

Several optogenetic approaches to restoration of sight have been tested, ranging from transfection of the ganglion cells [163], to bipolar cells [164] and even to surviving photoreceptor somas whose outer segments have degenerated [165]. Optogenetic stimulation of the retina currently requires very intense visible light (blue to yellow)—well beyond the natural range of vision—which is likely to be painfully bright and might be cytotoxic for patients even with only a few remaining photoreceptors. Efforts to shift opsin spectral sensitivities to longer wavelengths have recently been met with some success with the discovery of the Chrimson family of molecules [166]. However, the peak spectral sensitivity for these molecules is at 590 nm, i.e. still in the visible range.

Sensitivity of optogenetic stimulation is limited by 3 factors: the number of ion channels expressed on the cell membrane, the absorption coefficient of the chromophore, and the opening time of the ion channel. The longer a channel stays open after absorbing a photon, the more ions will get into the cell, so the less intense light will be required for stimulation. However, encoding precise temporal patterns in ganglion cells requires millisecond precision, and therefore short molecule response times, which limits their sensitivity [166]. Targeting bipolar cells or photoreceptor somas does not require such precise timing, but with opening times exceeding 50 ms the retinal response would be significantly slower than with natural vision (below 20 Hz). The fastest optogenetic probe reported to date (called the 'Chronos' molecule) can drive spiking at up to 60 Hz. However, its requirement of very bright light with peak spectral sensitivity around 500 nm makes it unsuitable for restoration of sight to patients with any residual vision.

Currently, the minimum light intensity required to drive retinal responses is on the order of 0.05–0.15 mW mm^{-2} at the spectral peak of sensitivity of the opsin molecule [166], which is above the natural range of retinal illumination (typically below 1 μW cm^{-2}). Therefore, optogenetic approaches will likely require video goggles to intensify light and help process the images prior to their projection onto the retina [52, 167]. One way to improve sensitivity would be to amplify opsin-driven ionic currents using G proteins, as it happens in photoreceptors. Such a significant alteration of cellular function has not yet been achieved.

5.2.2. Photoswitches. One major difficulty with clinical implementation of optogenetics is regulatory, since it requires permanent genetic modification of retinal neurons, with the inserted gene coming from a very remote organism—an algae. An alternative approach, which does not require gene therapy, is based on small light-sensitive molecules (so-called molecular switches) which bind to voltage-sensitive ion channels, thereby rendering them light sensitive [168, 169]. These molecules

injected into the vitreous humor partially restored light sensitivity in mice model of retinitis pigmentosa. However, since lifetime of these molecules in the body is only a few days, they would require frequent injections or sustained release. Within the irradiance levels similar to bright ambient illumination (1μW mm^{-2}), the kinetics of the retinal response to photoswitches are extremely slow (tens of seconds) [169]. They improve with more intense illumination, but acceptable response time is reached at irradiances of several mW mm^{-2}—three orders of magnitude above the upper end of natural illumination. The search for more sensitive photoswitches with absorption spectrums extending to longer wavelengths continues.

5.3. Mechanical stimulation

Neurons can be stimulated mechanically, and focused ultrasound is a potential noninvasive technology for interfacing with the nervous system. Spatial resolution is limited by the wavelength, which in turn, is limited by absorption and scattering in tissue. When focused into the brain through the highly scattering scull, frequencies below 1 MHz are preferred, making the focal spot size larger than 1 mm. Higher frequencies can be used for retinal stimulation: ultrasonic activation of the salamander retina has been demonstrated at 43 MHz, resulting in a focal spot of 90 μm in diameter [170].

5.4. Sensory substitution

Several sensory substitution systems for the visually impaired exist today [171]. Tactile-visual sensory substitution, first proposed in 1969 [172], included a two dimensional array of vibrating Teflon tips pressed against the back of the patient to form a pictorial display.

Another visual sensory substitution system converts images captured by a camera into electrical patterns on an array of microelectrodes placed on a tongue. The system, called BrainPort (Wicab, Inc, Madison, WI) includes 21×21 electrode array, and after extensive training, patients can localize and recognize objects, and sometimes even read words [173].

Visual information can also be converted into a sequence of sounds representing a raster scan of the image, with the local brightness encoded into the pitch and timbre as a function of lateral and vertical position in the image. Amplitude of the sound can be used to encode depth (axial distance from the patient). After training, patients can learn to localize objects and even demonstrate some object recognition capabilities [174, 175].

6. Outlook

We conclude this review by suggesting some perspectives for future advancement in the field.

6.1. Improving proximity to the target neurons

Proximity between the implant and the target cells becomes a limiting factor when electrode size is comparable to the target cell size, or when separation between the active and return electrodes is similar to the distance to the target cells [47, 51]. Since neurons in the INL are typically separated from a subretinal implant by 5–35 μm [99], it is difficult to foresee planar subretinal implants with local return electrodes and pixel pitch smaller than 35 μm elicit visual percepts at safe stimulation thresholds. To improve proximity between the stimulating electrodes and the target neurons, subretinal photodiode arrays could be integrated with pillar electrodes, which penetrate into the retina due to the migration of retinal tissue into the voids between pillars [46, 55] (see section 3.2.4). With close proximity, the electrode size is limited only by size of the cell soma, which is on the order of 10 μm. In addition to more selective stimulation and higher pixel density, improved proximity with 3 dimensional interfaces should reduce stimulation thresholds. However, 3 dimensional implants will be very difficult to explant, since the retina integrates into them, and careful biocompatibility and long-term stability studies will be required before they can be implanted in a patient.

6.2. Intracellular electrodes

Although pillar electrodes might help reduce pixel size, a paradigm shift might come with the use of intracellular microelectrodes. Hai *et al* demonstrated that electrodes can be internalized by neurons using their phagocytic response to subsellular-scale foreign bodies [176]. When cell engulfs a micrometer-sized electrode, rendering it membrane leaky at sharp edges, the electrode essentially becomes intracellular. Pt-tip electrodes with a hydrophobic band can also provide intracellular access to neurons [177], which could reduce stimulation thresholds by 4 orders of magnitude, and enable neural control using a graded variation of the electrode potential. In addition to single cell resolution, such interfaces would allow not only depolarization, but also hyperpolarization of the target cell, which would enable both stimulation and inhibition in the neurons of interest. This would likely help improve both resolution and contrast sensitivity. While intracellular electrodes seem to be well-tolerated in-vitro over a few weeks [176], this effect has not been demonstrated *in vivo* yet. It is unclear therefore what the long-term effects of intracellular access to a neuron are.

6.3. Image processing

Significant opportunities for improving the implant performance might come from more advanced image processing. Virtual and augmented reality devices are becoming commonplace, and computers are getting better at understanding the features of the visual world. Simplification of the visual scene prior its display on an implant may help better match its resolution and contrast sensitivity limits, and make visual percepts easier to understand. Several groups have already demonstrated promising results by segregating the visual content of a scene by distance, and displaying only the closer objects [178], or by encoding depth instead of luminance information to facilitate navigation [179].

6.4. Brain plasticity and the retinal code: how much fidelity do we need?

The need for complete and accurate restoration of the visual code is being actively debated. Proponents of subretinal implants argue that an implant providing high visual acuity and sufficient image contrast should be able to deliver meaningful visual percepts to patients, and they hope that the brain will be capable of learning a new prosthetic language, as long as the retinotopic map is preserved, contrast modulation is monotonic, and the signals are reproducible. Others, in favor of an epiretinal approach [116], argue that optimal performance of an implant will be attained only after the natural visual code is restored in each and every ganglion cell type. This debate is likely to continue until each type of implant is tested in patients, and behavioral performance is carefully assessed.

Acknowledgments

We would like to thank Dr L Grosberg for proof-reading the manuscript. Our contributions to this research were supported by the National Institutes of Health (grant R01-EY-018608), the Department of Defense (grant W81XWH-15-1-0009) and the Stanford Spectrum fund with grants to DP. GG was supported by a Stanford Neurosciences Institute Interdisciplinary Scholar Award.

References

[1] Smith W, Assink J, Klein R, Mitchell P, Klaver C C, Klein B E, Hofman A, Jensen S, Wang J J and de Jong P T 2001 Risk factors for age-related macular degeneration: pooled findings from three continents *Ophthalmology* **108** 697–704

[2] Bostock H 1983 The strength-duration relationship for excitation of myelinated nerve: computed dependence on membrane parameters *J. Physiol.* **341** 59–74

[3] McIntyre C C and Grill W M 1998 Sensitivity analysis of a model of mammalian neural membrane *Biol. Cybern.* **72** 29–37

[4] Spira M E and Hai A 2013 Multi-electrode array technologies for neuroscience and cardiology *Nat. Nanotechnol.* **8** 83–94

[5] Deuschl G *et al* 2006 A randomized trial of deep-brain stimulation for parkinson's disease *New Engl. J. Med.* **355** 896–908

[6] Eshraghi A A, Nazarian R, Telischi F F, Rajguru S M, Truy E and Gupta C 2012 The cochlear implant: historical aspects and future prospects *Anatomical Rec.* **295** 1967–80

[7] Zrenner E *et al* 2010 Subretinal electronic chips allow blind patients to read letters and combine them to words *Proc. R. Soc.* B **278** 1489–97

[8] Kessler T M *et al* 2007 Sacral neuromodulation for refractory lower urinary tract dysfunction: results of a nationwide registry in switzerland *Eur. Urol.* **51** 1357–63

[9] Brinton M, Chung J L, Kossler A, Kook K H, Loudin J, Franke M and Palanker D V 2015 Electronic enhancement of tear secretion *J. Neural Eng.* **13** 016006

[10] Greenberg R J, Velte T J, Humayun M S, Scarlatis G N and de Juan E Jr 1999 Computational model of electrical stimulation of the retinal ganglion cell *IEEE Trans. Biomed. Eng.* **46** 505–14

[11] Boinagrov D, Pangratz-Fuehrer S, Goetz G and Palanker D 2014 Selectivity of direct and network-mediated stimulation of the retinal ganglion cells with epi-, sub- and intra-retinal electrodes *J. Neural Eng.* **11** 026008

[12] Boinagrov D, Loudin J and Palanker D 2010 Strength-duration relationship for extracellular neural stimulation: numerical and analytical models *J. Neurophysiol.* **104** 2236–48

[13] Wandell B 1995 *Foundations of Vision* (Sunderland, MA: Sinauer Associates, Inc)

[14] Masland R H 2001 The fundamental plan of the retina *Nat. Neurosci.* **4** 877–86

[15] Heinz Wassle 2004 Parallel processing in the mammalian retina *Nat. Rev. Neurosci.* **5** 747–57

[16] Greschner M, Field G D, Li P H, Schiff M L, Gauthier J L, Ahn D, Sher A, Litke A M and Chichilnisky E J 2014 A polyaxonal amacrine cell population in the primate retina *J. Neurosci.* **34** 3597–606

[17] Baden T *et al* 2016 The functional diversity of retinal ganglion cells in the mouse *Nature* **529** 345–50

[18] Curcio C A and Allen K A 1990 Topography of ganglion cells in human retina *J. Comp. Neurol.* **300** 5–25

[19] Field G D, Sher A, Gauthier J L, Greschner M, Shlens J, Litke A M and Chichilnisky E J 2007 Spatial properties and functional organization of small bistratified ganglion cells in primate retina *J. Neurosci.* **27** 13261–72

[20] Salzman C D, Britten K H and Newsome W T 1990 Cortical microstimulation influences perceptual judgements of motion direction *Nature* **346** 174–7

[21] Britten K H, Shadlen M N, Newsome W T and Movshon J A 1992 The analysis of visual motion: a comparison of neuronal and psychophysical performance *J. Neurosci.* **12** 4745–65

[22] Merigan W H and Maunsell J H R 1993 How parallel are the primate visual pathways? *Annu. Rev. Neurosci.* **16** 369–402

[23] Barlow H B, Hill R M and Levick W R 1964 Retinal ganglion cells responding selectively to direction and speed of image motion in the rabbit *J. Physiol.* **173** 377–407

[24] Vaney D I, Sivyer B and Taylor W R 2012 Direction selectivity in the retina: symmetry and asymmetry in structure and function *Nat. Rev. Neurosci.* **13** 194–208

[25] Olveczky B P, Baccus S and Meister M 2003 Segregation of object and background motion in the retina *Nature* **423** 401–8

[26] Briggman K L, Helmstaedter M and Denk W 2011 Wiring specificity in the direction-selectivity circuit of the retina *Nature* **471** 183–90

[27] Haim M 2002 Epidemiology of retinitis pigmentosa in denmark *Acta Ophthalmol. Scand. Suppl.* **233** 1–34

[28] Grover S, Fishman G A, Anderson R J, Tozatti M S V, Heckenlively J R, Weleber R G, Edwards A O and Brown J Jr 1999 Visual acuity impairement in patients with retinitis pigmentosa at age 45 years and older *Ophthalmology* **106** 1780–5

[29] Humayun M S, Prince M, de Juan E, Barron Y, Moskowitz M, Klock I B and Milam A H 1999 Morphometric analysis of the extramacular retina from postmortem eyes with retinitis pigmentosa *Investigative Ophthalmol. Vis. Sci.* **40** 143–8

[30] Marc R E, Jones B W, Watt C B and Strettoi E 2003 Neural remodeling in retinal degeneration *Prog. Retinal Eye Res.* **22** 607–55

[31] Marc R E and Jones B W 2003 Retinal remodeling in inherited photoreceptor degenerations *Mol. Neurobiol.* **28** 139–47

[32] Jones B W and Marc R E 2005 Retinal remodeling during retinal degeneration *Exp. Eye Res.* **81** 123–37

[33] Ahuja A K, Dorn J D, Caspi A, McMahon M J, Dagnelie G, Dacruz L, Stanga P, Humayun M S, Greenberg R J and Argus II Study Group 2011 Blind subjects implanted with the Argus II retinal prosthesis are able to improve performance in a spatial-motor task *Br. J. Ophthalmol.* **95** 539–43

[34] Humayun M S *et al* and Argus II Study Group 2012 Interim results from the international trial of second sight's visual prosthesis *Ophthalmol.* **119** 779–88

[35] Stingl K, Bartz-Schmidt K-U, Gekeler F, Kusnyerik A, Sachs H and Zrenner E 2013 Functional outcome in subretinal electronic implants depends on foveal eccentricity *Investigative Ophthalmol. Vis. Sci.* **54** 7658–65

[36] Morimoto T *et al* 2011 Chronic implantation of newly developed suprachoroidal-transretinal stimulation prosthesis in dogs *Investigative Ophthalmol. Vis. Sci.* **52** 6785–92

[37] Ayton L *et al* and The Bionic Australia Research Consortium 2014 First-in-human trial of a novel suprachoroidal retinal prosthesis *PLoS One* **9** e115239

[38] Knutson J, Naples G, Peckham P and Keith M 2002 Electrode fracture rates and occurences of infection and granuloma associated with percutaneous intramuscular electrodes in upper-limb functional electrical stimulation applications *J. Rehabil. Res. Dev.* **39** 671–84

[39] Wang G, Liu W, Sivaprakasam M and Kendir G A 2005 Design and analysis of an adaptive transcutaneous power telemetry for biomedical implants *IEEE Trans. Circuits Syst.* **52** 2109–17

[40] Osepchuck J M 1983 *Biological Effects of Electromagnetic Radiation* (*IEEE Press Selected Reprint Series*) (New York: IEEE)

[41] Shannon C 1998 Communication in the presence of noise *Proc. IEEE* **86** 447–57

[42] Liu W, Vichienchom K, Clements M, DeMarco S C, Hughes C, McGucken E, Humayun M, de Juan E, Weiland J D and Greenberg R J 2000 A neuro-stimulus chip with telemetry unit for retinal prosthesis device *IEEE Solid-state Circuits* **35** 1487–97

[43] Naumann J 2012 *Search for Paradise: a Patient's Account of the Artificial Vision Experiment* (Bloomington, IN: Xlibris)

[44] Rizzo J F 3rd 2011 Update on retinal prosthetic research: the boston retinal implant project *J. Neuroophthalmol.* **31** 160–8

[45] Klauke S, Goertz M, Rein S, Hoehl D, Thomas U, Eckhorn R, Bremmer F and Wachtler T 2011 Stimulation with a wireless intraocular epiretinal implant elicits visual percepts in blind humans *Investigative Ophthalmol. Vis. Sci.* **52** 449–55

[46] Loudin J D, Simanovskii D M, Vijayraghavan K, Sramek C K, Butterwick A F, Huie P, McLean G and Palanker D V 2007 Optoelectronic retinal prosthesis: system design and performance *J. Neural Eng.* **4** S72–84

[47] Mathieson K *et al* 2012 Photovoltaic retinal prosthesis with high pixel density *Nat. Photon.* **6** 391–7

[48] Ghezzi D *et al* 2013 A polymer optoelectronic interface restores light sensitivity in blind rat retinas *Nat. Photon.* **7** 400–6

[49] Lorach H *et al* 2015 Photovoltaic restoration of sight with high visual acuity *Nat. Med.* **21** 476–82

[50] Chow A 1993 Electrical stimulation of the rabbit retina with subretinal electrodes and high density microphotodiode array implants *Investigative Ophthalmol. Vis. Sci.* **34** 835

[51] Palanker D, Vankov A, Huie P and Baccus S 2005 Design of a high-resolution optoelectronic retinal prosthesis *J. Neural Eng.* **2** S105–20

[52] Goetz G A, Mandel Y, Manivanh R, Palanker D V and Cizmar T 2013 Holographic display system for restoration of sight to the blind *J. Neural Eng.* **10** 056021

[53] Boinagrov D, Lei X, Goetz G, Kamins T, Mathieson K, Galambos L, Harris J and Palanker D V 2016 Photovoltaic pixels for neural stimulation: circuit models and performance *IEEE Trans. Biomed. Circuits Syst.* **10** 85–97

[54] Lee D Y, Lorach H, Huie P and Palanker D 2016 Implantation of modular photovoltaic subretinal prosthesis *Ophthalmic Surg. Lasers Imaging Retina* **47** 171–4

[55] Butterwick A, Huie P, Jones B W, Marc R E, Marmor M and Palanker D 2009 Effect of shape and coating of a subretinal prosthesis on its integration with the retina *Exp. Eye Res.* **88** 22–9

[56] Pardue M T, Stubbs E B Jr, Perlman J I, Narfstr K, Chow A Y and Peachey N S 2001 Immunohistochemical studies of the retina following long-term implantationwith subretinal microphotodiode arrays *Exp. Eye Res.* **73** 333–43

[57] Adekunle A N, Adkins A, Wang W, Kaplan H J, de Castro J F, Lee S J, Huie P, Palanker D, McCall M and Pardue M T 2015 Integration of perforated subretinal prostheses with retinal tissue *Trans. Vis. Sci. Technol.* **4** 5

[58] Anderson D J, Najafi K, Tanghe S J, Evans D A, Levy K L, Hetke J F, Xue X L, Zappia J J and Wise K D 1989 Batch-fabricated thin-film electrodes for stimulation of the central auditory system *IEEE Trans. Biomed. Eng.* **36** 693–704

[59] Weiland J D and Anderson D J 2000 Chronic neural stimulation with thin-film, iridium oxide electrodes *IEEE Trans. Biomed. Eng.* **47** 911–8

[60] Loeb G E, Bak M J, Salcman M and Schmidt E M 1977 Parylene as a chronically stable, reproducible microelectrode insulator *IEEE Trans. Biomed. Eng.* **24** 121–8

[61] Hsu J M, Rieth L, Normann R A, Tathireddy P and Solzbacher F 2009 Encapsulation of an integrated neural interface device with parylene c *IEEE Trans. Biomed. Eng.* **56** 23–9

[62] Kane S R, Cogan S F, Ehrlich J, Plante T D, McCreery D B and Troyk P R 2013 Electrical performance of penetrating microelectrodes chronically implanted in cat cortex *IEEE Trans. Biomed. Eng.* **60** 2153–60

[63] Potts S E *et al* 2011 Ultra-thin aluminium oxide films deposited by plasma-enhanced atomic layer deposition for corrosion protection *J. Electrochem. Soc.* **158** C132

[64] Hadjinicolaou A E *et al* 2012 Electrical stimulation of retinal ganglion cells with diamond and the development of an all diamond retinal prosthesis *Biomaterials* **33** 5812–20

[65] Roy R K and Lee K R 2007 Biomedical applications of diamond-like carbon coatings: a review *J. Biomed. Mater. Res. B: Appl. Biomater.* **83** 72–84

[66] Xiao X *et al* 2006 *In vitro* and *in vivo* evaluation of ultrananocrystalline diamond for coating of implantable retinal microchips *J. Biomed. Mater. Res. B: Appl. Biomater.* **77** 273–81

[67] Bolz A, Amon M, Ozbek C, Heublein B and Schaldach M 1996 Coating of cardiovascular stents with a semiconductor to improve their hemocompatibility *Tex. Heart Inst. J.* **23** 162–6

[68] Bendali A, Agnes C, Meffert S, Forster V, Bongrain A, Arnault J C, Sahel J A, Offenhausser A, Bergonzo P and Picaud S 2014 Distinctive glial and neuronal interfacing on nanocrystalline diamond *PLoS One* **9** e92562

[69] Lei X, Kane S, Cogan S, Lorach H, Galambos L, Huie P, Mathieson K, Kamins T, Harris J and Palanker D 2016 SiC protective coating for photovoltaic retinal prostheses *J. Neural Eng.* **3** 046016

[70] Sramek C, Paulus Y, Nomoto H, Huie P, Brown J and Palanker D 2009 Dynamics of retinal photocoagulation and rupture *J. Biomed. Opt.* **14** 034007

[71] Delori F C, Webb R H and Sliney D H 2007 Maximum permissible exposures for ocular safety (ANSI 2000), with emphasis on ophthalmic devices *J. Opt. Soc. Am.* **24** 1250–65

[72] Lorach H, Wang J, Lee D Y, Dalal R, Huie P and Palanker D 2016 Retinal safety of near infrared radiation in photovoltaic restoration of sight *Biomed. Opt. Express* **7** 13–21

[73] McCreery D B, Agnew W F, Yuen T G and Bullara L 1990 Charge density and charge per phase as cofactors in neural injury induced by electrical stimulation *IEEE Trans. Biomed. Eng.* **37** 996–1001

[74] Neumann E 1992 Membrane electroporation and direct gene-transfer *Bioelectrochem. Bioenerg.* **28** 247–67

[75] Butterwick A F, Vankov A, Huie P, Freyvert Y and Palanker D V 2007 Tissue damage by pulsed electrical stimulation *IEEE Trans. Biomed. Eng.* **54** 2261–7

[76] Jensen R J, Rizzo J F, Ziv O R, Grumet A and Wyatt J 2003 Thresholds for activation of rabbit retinal ganglion cells with an ultrafine, extracellular microelectrode *Investigative Ophthalmology. Vis. Sci.* **44** 3533–43

[77] Jensen R J, Ziv O R and Rizzo J F 2005 Responses of rabbit retinal ganglion cells to electrical stimulation with an epiretinal electrode *J. Neural Eng.* **2** S16–21

[78] Robblee L S and Rose T L 1990 Electrochemical guidelines for selection of protocols and electrode materials for neural stimulation *Neural Prostheses: Fundamental Studies* (Englewood Cliffs, NJ: Prentice Hall)

[79] Merrill D R, Bikson M and Jefferys J G 2005 Electrical stimulation of excitable tissue: design of efficacious and safe protocols *J. Neurosci. Methods* **141** 171–98

[80] Cogan S F 2008 Neural stimulation and recording electrodes *Annu. Rev. Biomed. Eng.* **10** 275–309

[81] Weiland J, Anderson D J and Humayun M 2002 *In vitro* electrical properties for iridium oxide versus titanium nitride stimulating electrodes *IEEE Trans. Biomed. Eng.* **49** 1574–9

[82] Helmstaedter M, Briggman K L, Turaga S C, Jain V, Seung H S and Denk W 2013 Connectomic reconstruction of the inner plexiform layer in the mouse retina *Nature* **500** 168–74

[83] Chichilnisky E J and Kalmar R S 2002 Functional asymmetries in on and off ganglion cells of primate retina *J. Neurosci.* **22** 2737–47

[84] Devries S H and Baylor D A 1997 Mosaic arrangement of ganglion cell receptive fields in rabbit retina *J. Neurophysiol.* **78** 2048–60

[85] Enroth-Cugell C and Robson J G 1966 The contrast sensitivity of retinal ganglion cells of the cat *J. Physiol.* **187** 517–52

[86] Chen S J, Mahadevappa M, Roizenblatt R, Weiland J and Humayun M 2006 Neural responses elicited by electrical stimulation of the retina *Trans. Am. Ophthalmol. Soc.* **104** 252–9

[87] Humayun M, Propst R, de Juan E, McCormick K and Hickingbotham D 1994 Bipolar surface electrical stimulation of the vertebrate retina *Arch. Ophthalmol.* **112** 110–6

[88] O'Hearn T M, Sadda S R, Weiland J, Maia M, Margalit E and Humayun M 2006 Electrical stimulation in normal and retinal degeneration (RD1) isolated mouse retina *Vis. Res.* **46** 3198–204

[89] Sekirnjak C, Hulse C, Jepson L H, Hottowy P, Sher A, Dabrowski W, Litke A M and Chichilnisky E J 2009 Loss of responses to visual but not electrical stimulation in ganglion cells of rats with severe photoreceptor degeneration *J. Neurophysiol.* **102** 3260–9

[90] Cho A, Ratliff C, Sampath A and Weiland J 2016 Changes in ganglion cell physiology during retinal degeneration influence excitability by prosthetic electrodes *J. Neural Eng.* **13** 025001

[91] Margolis D J, Newkirk G, Euler T and Detwiler P B 2008 Functional stability of retinal ganglion cells after degeneration-induced changes in synaptic input *J. Neurosci.* **28** 6526–36

[92] Sekirnjak C, Jepson L H, Hottowy P, Sher A, Dabrowski W, Litke A M and Chichilnisky E J 2011 Changes in physiological properties of rat ganglion cells during retinal degeneration *J. Neurophysiol.* **105** 2560–71

[93] Menzler J and Zeck G 2011 Network oscillations in rod-degenerated mouse retinas *J. Neurosci.* **31** 2280–91

[94] Nassi J J and Callaway E M 2009 Parallel processing strategies of the primate visual system *Nat. Rev. Neurosci.* **10** 360–72

[95] Huberman A D and Niell C M 2011 What can mice tell us about how vision works? *Trends Neurosci.* **34** 464–73

[96] Zoccolan D 2015 Invariant visual object recognition and shape processing in rats *Behav. Brain Res.* **285** 10–33

[97] Strauss O, Stumpff F, Mergler S, Wienrich M and Wiederholt M 1998 The royal college of surgeons rat: an animal model for inhereted retinal degeneration with a still unknown genetic defect *Acta Anatomica* **162** 101–11

[98] Peng Y W, Senda T, Hao Y, Matsuno K and Wong F 2003 Ectopic synaptogenesis during retinal degeneration in the royal college of surgeons rat *Neuroscience* **119** 813–20

[99] Mandel Y *et al* 2013 Cortical responses elicited by photovoltaic subretinal prostheses exhibit similarities to visually evoked potentials *Nat. Commun.* **4** 1980

[100] Shen J, Yang X, Dong A, Petters R M, Peng Y W, Wong F and Campochiaro P A 2005 Oxidative damage is a potential cause of cone cell death in retinitis pigmentosa *J. Cell Physiol.* **203** 457–64

[101] Chang B, Hawes N L, Hurd R E, Davisson M T, Nusinowitz S and Heckenlively J R 2002 Retinal degeneration mutants in the mouse *Vis. Res.* **42** 517–25

[102] Lorach H, Kung J, Beier C, Mandel Y, Dalal R, Huie P, Wang J, Lee S, Sher A, Jones B W and Palanker D 2015 Development of animal models of local retinal degeneration *Investigative Ophthalmol. Vis. Sci.* **56** 4644–52

[103] Lorach H, Lei X, Galambos L, Kamins T, Mathieson K, Dalal R, Huie P, Harris J and Palanker D 2015 *Investigative Ophthalmology and Visual Science* **56** 7444–50

[104] Lapicque L 1907 Recherches quantitatives sur l'excitation éltrique des nerfs traitée comme une polarisation *J. Physiol. Pathol. Gen.* **9** 620–35

[105] Weiss G 1901 Sur la possibilite de rendre comparables entre eux les appareils servant à l'excitation électrique *Arch. Ital. Biol.* **35** 413–46

[106] Malmivuo J and Plonsey R 1995 *Bioelectromagnetism: Principles and Applications of Bioelectric and Biomagnetic Fields* (Oxford: Oxford University Press)

[107] Fried S I, Hsueh H A and Werblin F S 2006 A method for generating precise temporal patterns of retinal spiking using prosthetic stimulation *J. Neurophysiol.* **95** 970–8

[108] Jensen R J and Rizzo J F 2006 Thresholds for activation of rabbit retinal ganglion cells with a subretinal electrode *Exp. Eye Res.* **83** 367–73

[109] Lorach H, Goetz G, Mandel Y, Lei X, Kamins T I, Mathieson K, Huie P, Dalal R, Harris J S and Palanker D 2014 Performance of photovoltaic arrays *in vivo* and characteristics of prosthetic vision in animals with retinal degeneration *Vis. Res.* **111** 142–8

[110] Flores T, Goetz G, Lei X and Palanker D 2016 Optimization of return electrodes in neurostimulating arrays *J. Neural Eng.* **13** 036010

[111] Bendali A *et al* 2015 Synthetic 3d diamond-based electrodes for flexible retinal neuroprostheses: model, production and *in vivo* biocompatibility *Biomaterials* **67** 73–83

[112] Suzuki S, Humayun M, Weiland J, Chen E Y, Margalit E, Piyathaisere D V and de Juan E 2004 Comparison of electrical stimulation thresholds in normal and retinal degenerated mouse retina *Japan. J. Ophthalmol.* **48** 345–9

[113] Sekirnjak C, Hottowy P, Sher A, Dabrowski W, Litke A M and Chichilnisky E J 2006 Electrical stimulation of mammalian retinal ganglion cells with multielectrode arrays *J. Neurophysiol.* **95** 3311–27

[114] Jepson L H, Hottowy P, Mathieson K, Gunning D E, Dabrowski W, Litke A M and Chichilnisky E J 2013 Focal electrical stimulation of major ganglion cell types in the primate retina for the design of visual prostheses *J. Neurosci.* **33** 7194–205

[115] Fried S I, Lasker A C, Desai N J, Eddington D K and Rizzo J F 3rd 2009 Axonal sodium-channel bands shape the response to electric stimulation in retinal ganglion cells *J. Neurophysiol.* **101** 1972–87

[116] Jepson L H, Hottowy P, Weiner G A, Dabrowski W, Litke A M and Chichilnisky E J 2014 High-fidelity reproduction of spatiotemporal visual signals for retinal prosthesis *Neuron* **83** 87–92

[117] Cai C, Ren Q, Desai N J, Rizzo J F 3rd and Fried S I 2011 Response variability to high rates of electric stimulation in retinal ganglion cells *J. Neurophysiol.* **106** 153–62

[118] Weitz A C *et al* 2015 Improving the spatial resolution of epiretinal implants by increasing stimulus pulse duration *Sci. Trans. Med.* **16** 318ra203

[119] Behrend M R, Ahuja A K, Humayun M S, Chow R H and Weiland J D 2011 Resolution of the epiretinal prosthesis is not limited by electrode size *IEEE Trans. Neural Syst. Rehabil. Eng.* **19** 436–42

[120] Freeman D K and Fried S I 2011 Multiple components of ganglion cell desensitization in response to prosthetic stimulation *J. Neural Eng.* **8** 016008

[121] Lee S W, Eddington D K and Fried S I 2013 Responses to pulsatile subretinal electric stimulation: effects of amplitude and duration *J. Neurophysiol.* **109** 1954–68

[122] Tsai D, Morley J W, Suaning G J and Lovell N H 2009 Direct activation and temporal response properties of rabbit retinal ganglion cells following subretinal stimulation *J. Neurophysiol.* **102** 2982–93

[123] Jensen R J and Rizzo J F 2007 Responses of ganglion cells to repetitive electrical stimulation of the retina *J. Neural Eng.* **4** S1–6

[124] Goetz G, Smith R, Lei X, Galambos L, Kamins T, Mathieson K, Sher A and Palanker D V 2015 Contrast sensitivity with a subretinal prosthesis and implications for efficient delivery of visual information *Investigative Ophthalmol. Vis. Sci.* **56** 7186–94

[125] Newsome W T, Wurtz R H, Dursteler M R and Mikami A 1985 Deficits in visual motion processing following lbotenic acid lesions of the middle temporal visual area of the macaque monkey *J. Neurosci.* **5** 825–40

[126] You Y, Klistorner A, Thie J and Graham S 2011 Latency delay of visual evoked potential is a real measurement of demyelination in a rat model of optic neuritis *Investigative Ophthalmol. Vis. Sci.* **52** 6911–8

[127] Rossi E A and Roorda A 2010 The relationship between visual resolution and cone spacing in the human fovea *Nat. Neurosci.* **13** 156–7

[128] Li P H, Gauthier J L, Schiff M, Sher A, Ahn D, Field G D, Greschner M, Callaway E M, Litke A M and Chichilnisky E J 2015 Anatomical identification of extracellularly recorded cells in large-scale multielectrode recordings *J. Neurosci.* **35** 4663–75

[129] Richard E, Goetz G and Chichilnisky E J 2015 Recognizing retinal ganglion cells in the dark *Adv. Neural Inf. Process. Syst.* **28** 2467–75

[130] Kolb H and Marshak D 2003 The midget pathways of the primate retina *Doc. Ophthalmol.* **2003** 67–81

[131] Sim S L, Szalewski R J, Johnson L J, Akah L E, Shoemaker L E, Thoreson W B and Margalit E 2014 Simultaneous recording of mouse retinal ganglion cells during epiretinal or subretinal stimulation *Vis. Res.* **101** 41–50

[132] Harnois C, Bodis-Wollner I and Onofrj M 1984 The effect of contrast and spatial frequency on the visual evoked potential of the hooded rat *Exp. Brain Res.* **57** 1–8

[133] Thibos L N and Levick W R 1983 Bimodal receptive fields of cat retinal ganglion cells *Vis. Res.* **23** 1561–72

[134] Passaglia C L, Troy J B, Ruttiger L and Lee B B 2002 Orientation sensitivity of ganglion cells in primate retina *Vis. Res.* **42** 683–94

[135] Brown S P, He S and Masland R H 2000 Receptive field microstructure and dendritic geometry of retinal ganglion cells *Neuron* **27** 371–83

[136] Caldwell J H and Daw N W 1978 New properties of rabbit retinal ganglion cells *J. Physiol.* **276** 257–76

[137] Demb J B, Haarsma L, Freed M A and Sterling P 1999 Functional circuitry of the retinal ganglion cell's nonlinear receptive field *J. Neurosci.* **19** 9756–67

[138] Petrusca D, Grivich M I, Sher A, Field G D, Gauthier J L, Greschner M, Shlens J, Chichilnisky E J and Litke A M 2007 Identification and characterization of a y-like primate retinal ganglion cell type *J. Neurosci.* **27** 11019–27

[139] Schwartz G W, Okawa H, Dunn F A, Morgan J L, Kerschensteiner D, Wong R O and Rieke F 2012 The spatial structure of a nonlinear receptive field *Nat. Neurosci.* **15** 1572–80

[140] Victor J D and Shapley R M 1979 The nonlinear pathway of y ganglion cells in the cat retina *J. Gen. Physiol.* **74** 671–89

[141] Borghuis B G, Marvin J S, Looger L L and Demb J B 2013 Two-photon imaging of nonlinear glutamate release dynamics at bipolar cell synapses in the mouse retina *J Neurosci* **33** 10972–85

[142] Silveira L C L, Heywood C A and Cowey A 1987 Contrast sensitivity and visual acuity of the pigmented rat determined electrophysiologically *Vis. Res.* **27** 1719–31

[143] Dean P 1981 Visual pathways and acuity in hooded rats *Behav. Brain Res.* **3** 239–71

[144] Shapley R M 1997 Retinal physiology: adapting to the changing scene *Curr. Biol.* **7** R412–23

[145] Kuang X, Poletti M, Victor J D and Rucci M 2012 Temporal encoding of spatial information during active visual fixation *Curr. Biol.* **22** 510–4

[146] Cohen E and Lepri B 2013 Investigational device exemption guidance for retinal prostheses Center for Devices and Radiological Health, Food and Drug Administration

[147] Ho A C *et al* and Argus II Study Group 2015 Long-term results from an epiretinal prosthesis to restore sight to the blind *Ophthalmology* **122** 1547–54

[148] Weiland J D and Humayun M S 2005 Retinal prosthesis *Ann. Rev. Biomed. Eng.* **7** 361–401

[149] da Cruz L *et al* and The Argus II Study Group 2013 The ARGUS II epiretinal prosthesis system allows letter and word reading and long-term function in patients with profound vision loss *Br. J. Ophthalmol.* **67** 632–6

[150] Garcia S, Petrini K, da Cruz L, Rubin G S and Nardini M 2014 Assessing improvements in perception afforded by retinal prostheses in multisensory tasks *Investigative Ophthalmol. Vis. Sci.* **55** 5962

[151] Nanduri D, Fine I, Horsager A, Boynton G M, Humayun M S, Greenberg R J and Weiland J D 2012 Frequency and amplitude modulation have different effects on the percepts elicited by retinal stimulation *Investigative Ophthalmol. Vis. Sci.* **53** 205–14

[152] Stingl K *et al* 2013 Artificial vision with wirelessly powered subretinal electronic implant alpha-ims *Proc. Biol. Sci.* **280** 20130077

[153] Hafed Z M, Stingl K, Bartz-Schmidt K U, Gekeler F and Zrenner E 2016 Oculomotor behavior of blind patients seeing with a subretinal visual implant *Vis. Res.* **118** 119–31

[154] Fujikado T *et al* 2011 Testing of semichronically implanted retinal prosthesis by suprachoroidal-transretinal stimulation in patients with retinitis pigmentosa *Investigative Ophthalmol. Vis. Sci.* **52** 4726–33

[155] Chow A, Chow V, Packo K, Pollack J, Peyman G and Schuchard R 2004 The artificial silicon retina microchip for the treatment of vision loss from retinitis pigmentosa *Arch. Ophthalmol.* **122** 460–9

[156] Veraart C, Delbeke D, Wanet-Defalque M C, Vanlierde A, Michaux G, Parrini S, Glineur O, Verleysen M, Trullemans C and Mortimer J T 1999 Selective stimulation of the human optic nerve *4th Annual Conf. of the Int. Functional Electrical Stimulation Society* pp 57–9
[157] Chai X, Li L, Wu K, Zhou C, Cao P and Ren Q 2008 C-sight visual prostheses for the blind *IEEE Eng. Med. Biol. Mag.* **27** 20–8
[158] Pezaris J S and Reid R C 2007 Demonstration of artificial visual percepts generated through thalamic microstimulation *Proc. Natl Acad. Sci. USA* **104** 7670–5
[159] Wiesel T N and Hubel D H 1966 Spatial and chromatic interactions in the lateral geniculate body of the rhesus monkey *J. Neurophysiol.* **29** 1115–56
[160] Brindley G S and Lewin W S 1968 The sensations produced by electrical stimulation of the visual cortex *J. Physiol.* **196** 479–93
[161] Murphey D K, Maunsell J H R, Beauchamp M S and Yoshor D 2009 Perceiving electrical stimulation of identified human visual areas *Proc. Natl Acad. Sci. USA* **106** 5389–93
[162] Yizhar O, Fenno L E, Davidson T J, Mogri M and Deisseroth K 2011 Optogenetics in neural systems *Neuron* **71** 9–34
[163] Tomita H *et al* 2009 Visual properties of transgenic rats harboring the channelrhodopsin-2 gene regulated by the thy-1.2 promoter *PLoS One* **4** e7679
[164] Lagali P S, Balya D, Awatramani G B, Munch T A, Kim D S, Busskamp V, Cepko C L and Roska B 2008 Light-activated channels targeted to on bipolar cells restore visual function in retinal degeneration *Nat. Neurosci.* **11** 667–75
[165] Busskamp V *et al* 2010 Genetic reactivation of cone photoreceptors restores visual responses in retinitis pigmentosa *Science* **329** 413–7
[166] Klapoetke N C *et al* 2014 Independent optical excitation of distinct neural populations *Nat. Methods* **11** 338–46
[167] Reutsky-Gefen I, Golan L, Farah N, Schejter A, Tsur L, Brosh I and Shoham S 2013 Holographic optogenetic stimulation of patterned neuronal activity for vision restoration *Nat. Commun.* **4** 1509
[168] Polosukhina A *et al* 2012 Photochemical restoration of visual responses in blind mice *Neuron* **75** 271–82
[169] Tochitsky I, Polosukhina A, Degtyar V E, Gallerani N, Smith C M, Friedman A, van Gelder R N, Trauner D, Kaufer D and Kramer R H 2014 Restoring visual function to blind mice with a photoswitch that exploits electrophysiological remodeling of retinal ganglion cells *Neuron* **81** 800–13
[170] Menz M D, Oralkan O, Khuri-Yakub P T and Baccus S A 2013 Precise neural stimulation in the retina using focused ultrasound *J. Neurosci.* **33** 4550–60
[171] Bach-y Rita P and Kercel S W 2003 Sensory substitution and the human–machine interface *Trends Cogn. Sci.* **7** 541–6
[172] Bach-Y-Rita P, Collins C, Saunders F A, White B and Scadden L 1969 Vision substitution by tactile image projection *Nature* **221** 963–4
[173] Nau A C, Pintar C, Arnoldussen A and Fisher C 2015 Acquisition of visual perception in blind adults using the brainport artificial vision device *Am. J. Occup. Ther.* **69** 6901290010
[174] Capelle C, Trullemans C, Arno P and Verrart C 1998 A real-time experimental prototype for enhancement of vision rehabilitation using auditory substitution *IEEE Trans. Biomed. Eng.* **45** 1279–93
[175] Striem-Amit E, Cohen L, Dehaene S and Amedi A 2012 Reading with sounds: sensory substitution selectively activates the visual word form area in the blind *Neuron* **76** 640–52
[176] Hai A, Shappir J and Spira M E 2010 Long-term, multisite, parallel, in-cell recording and stimulation by an array of extracellular microelectrodes *J. Neurophysiol.* **104** 559–68
[177] Verma P and Melosh N A 2010 Gigaohm resistance membrane seals with stealth probe electrodes *Appl. Phys. Lett.* **97** 033704
[178] Jung J H, Aloni D, Yitzhaky Y and Peli E 2015 Active confocal imaging for visual prostheses *Vis. Res.* **111** 182–96
[179] Hicks S L, Wilson I, van Rheede J J, MacLaren R E, Downes S M and Kennard C 2014 Improved mobility with depth-based residual vision glasses *Investigative Ophthalmol. Vis. Sci.* **55** 2153